



HAL
open science

Role for Atlantic inflows and sea ice loss on shifting phytoplankton blooms in the Barents Sea

Laurent Oziel, Griet Neukermans, Mathieu Ardyna, Christiane Lancelot, Jean-Louis Tison, P. Wassmann, Jérôme Sirven, Diana Ruiz-Pino, Jean-Claude Gascard

► **To cite this version:**

Laurent Oziel, Griet Neukermans, Mathieu Ardyna, Christiane Lancelot, Jean-Louis Tison, et al.. Role for Atlantic inflows and sea ice loss on shifting phytoplankton blooms in the Barents Sea. *Journal of Geophysical Research. Oceans*, 2017, 122 (6), pp.5121 - 5139. 10.1002/2016JC012582 . hal-01644551

HAL Id: hal-01644551

<https://hal.science/hal-01644551v1>

Submitted on 18 Mar 2021

HAL is a multi-disciplinary open access archive for the deposit and dissemination of scientific research documents, whether they are published or not. The documents may come from teaching and research institutions in France or abroad, or from public or private research centers.

L'archive ouverte pluridisciplinaire **HAL**, est destinée au dépôt et à la diffusion de documents scientifiques de niveau recherche, publiés ou non, émanant des établissements d'enseignement et de recherche français ou étrangers, des laboratoires publics ou privés.

RESEARCH ARTICLE

10.1002/2016JC012582

Special Section:

The Arctic: An AGU Joint Special Collection

Key Points:

- A 17 year time-series of remotely sensed and in situ observations is used to describe the variability of phytoplankton blooms
- At least three distinct blooms were revealed and are partly controlled by the position of the sea ice edge and the polar front
- A north-eastward shift of the spring and summer blooms was observed

Supporting Information:

- Supporting Information S1
- Figure S1
- Figure S2
- Figure S3
- Figure S4

Correspondence to:

Laurent Oziel,
laurent.oziel@takuvik.ulaval.ca

Citation:

Oziel, L., G. Neukermans, M. Ardyna, C. Lancelot, J-L. Tison, P. Wassmann, J. Sirven, D. Ruiz-Pino, and J-C. Gascard (2017), Role for Atlantic inflows and sea ice loss on shifting phytoplankton blooms in the Barents Sea, *J. Geophys. Res. Oceans*, 122, 5121–5139, doi:10.1002/2016JC012582.








Received 28 NOV 2016

Accepted 9 MAY 2017

Accepted article online 16 MAY 2017

Published online 26 JUN 2017

Role for Atlantic inflows and sea ice loss on shifting phytoplankton blooms in the Barents Sea

L. Oziel^{1,2} , G. Neukermans^{2,3} , M. Ardyna³ , C. Lancelot⁴, J-L. Tison⁵ , P. Wassmann⁶ , J. Sirven¹, D. Ruiz-Pino¹ , and J-C. Gascard¹ 

¹Sorbonne Universités (UPMC, Univ Paris 06)-CNRS-IRD-MNHN, LOCEAN Laboratory, IPSL, Université Pierre et Marie Curie, Paris, France, ²Takuvik Joint International Laboratory, Laval University (Canada) – CNRS (France), UMI3376, Département de biologie et Québec-Océan, Université Laval, Québec, Québec, Canada, ³Sorbonne Universités, UPMC Univ Paris 06, INSU-CNRS, Laboratoire d’Océanographie de Villefranche, Villefranche-sur-mer, France, ⁴Laboratoire d’Ecologie des Systèmes Aquatiques, Université Libre de Bruxelles, Brussels, Belgium, ⁵Laboratoire de Glaciologie, DGES, Université Libre de Bruxelles, Brussels, Belgium, ⁶Faculty of Biosciences, Fisheries and Economy, Institute of Arctic and Marine Biology, UiT – The Arctic University of Norway, Tromsø, Norway

Abstract Phytoplankton blooms in the Barents Sea are highly sensitive to seasonal and interannual changes in sea ice extent, water mass distribution, and oceanic fronts. With the ongoing increase of Atlantic Water inflows, we expect an impact on these blooms. Here, we use a state-of-the-art collection of in situ hydrogeochemical data for the period 1998–2014, which includes ocean color satellite-derived proxies for the biomass of calcifying and noncalcifying phytoplankton. Over the last 17 years, sea ice extent anomalies were evidenced having direct consequences for the spatial extent of spring blooms in the Barents Sea. In years of minimal sea ice extent, two spatially distinct blooms were clearly observed: one along the ice edge and another in ice-free water. These blooms are thought to be triggered by different stratification mechanisms: heating of the surface layers in ice-free waters and melting of the sea ice along the ice edge. In years of maximal sea ice extent, no such spatial delimitation was observed. The spring bloom generally ended in June when nutrients in the surface layer were depleted. This was followed by a stratified and oligotrophic summer period. A coccolithophore bloom generally developed in August, but was confined only to Atlantic Waters. In these same waters, a late summer bloom of noncalcifying algae was observed in September, triggered by enhanced mixing, which replenishes surface waters with nutrients. Altogether, the 17 year time-series revealed a northward and eastward shift of the spring and summer phytoplankton blooms.

1. Introduction

The hydrography and dynamics of the Barents Sea are some of the best-known among Arctic shelf seas owing to numerous in situ observations that have been collected over the last several decades. The warm and saline Atlantic Water flows through the Nordic Seas into the Barents Sea opening (Figure 1) and invades the southwestern part of the Barents Sea bordering the warm and fresh Norwegian Coastal Current Water. At the Polar Front, Atlantic Water meets the cold and fresh Arctic Water flowing from the Nansen Basin. West of 32°E, the position of the Polar Front is well-described and stable as it is largely controlled by bottom topography [e.g., Loeng, 1991]. East of 32°E, the Polar Front splits into two branches: the “Southern Front,” associated with strong temperature gradients, and the “Northern Front,” associated with strong salinity gradients [Oziel *et al.*, 2016]. These dynamic fronts enclose the dense Barents Sea Water (Figure 1) and their position shows a strong interannual variability [Oziel *et al.*, 2016].

The impacts of climate change are particularly evident in the Arctic, where warming is two times faster than the global mean [Serreze and Barry, 2011]. The Barents Sea, like the other marginal seas of the Arctic Ocean, is particularly affected. The winter sea ice extent decreased by about 50% from 1998 to 2008 and has been partly attributed to an increase of the Atlantic Water inflow, referred to an “Atlantification” of the Barents Sea [Årthun *et al.*, 2012]. Recently, Polyakov *et al.* [2017] evidenced the increasing role of this “Atlantification” on sea ice loss in the Eurasian basin of the Arctic Ocean. Water budgets estimate 30–40% the Atlantic Water surface expansion in the Barents Sea over the last decade [Dalpadado *et al.*, 2012; Johannesen *et al.*, 2012]. However, based on the most extensive hydrographical in situ data set available to date, Oziel *et al.* [2016]

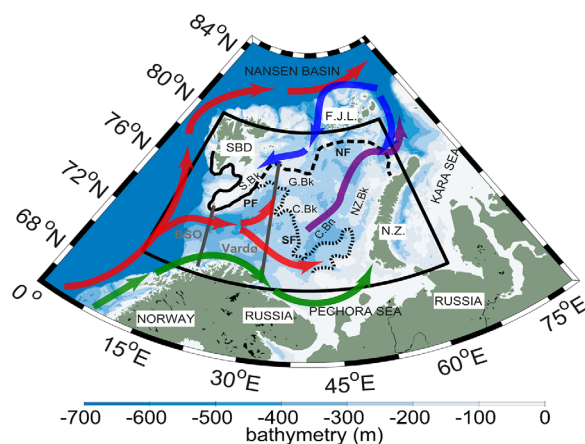


Figure 1. Barents Sea map with bathymetry. The black shape delimits the study area. Barents Sea Opening (BSO) and Vardø hydrographical sections are shown in gray. Circulation of the main water masses is depicted by the arrows (Atlantic water: red; Arctic water: blue; Norwegian Coastal Current: green; Barents Sea Waters: purple). Polar Front (PF, solid line), Southern Front (SF, dotted line), and Northern Front (NF, dashed line). SBD = Svalbard, F.J.L. = Franz Josef Land, N.Z. = Novaya Zemlya, S.Bk = Svalbard Bank, G.Bk = Great Bank, C.Bk = Central Bank, C.Bn = Central Basin.

[Wassmann *et al.*, 2006]. The Barents Sea bloom is also characterized by a high diversity, with up to 201 algae species [Rat'kova and Wassmann, 2002]. Among these, three main phytoplankton functional types with distinct roles in biogeochemical cycling and environmental or nutrient requirements [Le Quéré *et al.*, 2005] are commonly observed: diatoms as silicifiers (e.g., *Chaetoceros spp.*, *Nitzschia spp.*, *Thalassiosira spp.*), *Phaeocystis* (*P. pouchetii*) as producers of Dimethylsulfoniopropionate (DMSP), and coccolithophores (viz., *Emiliania huxleyi*, *Ehux.*) as calcifiers and DMSP producers.

The relative abundance of these phytoplankton functional types defines the typical phytoplankton phenology in the open waters of the Barents Sea. An intense spring bloom typically peaks in May and is mainly composed of diatoms and *P. pouchetii* whose relative abundance varies stochastically among years, but varies little within the Barents Sea for a given year [Degerlund and Eilertsen, 2010]. A summer bloom, dominated by the coccolithophore *Ehux.*, typically grows in August in a stratified nutrient-depleted water column [Smyth *et al.*, 2004; Signorini and McClain, 2009]. These phytoplankton blooms associated with calcifiers in summer and noncalcifiers in spring can be easily detected and differentiated from each other using satellite ocean color data of particulate inorganic carbon (PIC) and chlorophyll *a* (Chl *a*) concentrations, respectively [Signorini and McClain, 2009].

The environmental factors that control these phytoplankton blooms have been investigated previously using climatologies of ocean color remote sensing and hydrographic data [Signorini and McClain, 2009]. In the southwestern Barents Sea, the spring bloom starts in March–April with the increase of photosynthetically available radiation (PAR), sea surface temperature (SST), and a concomitant decrease of the mixed layer depth (MLD) due to thermal stratification. In the northern Barents Sea, partially ice-covered in winter, a phytoplankton spring bloom also develops when the sea ice begins to melt and forms a stable shallow Mixed Layer allowing optimal light and nutrient conditions and preventing phytoplankton from vertical excursions out of the euphotic layer [Sakshaug and Skjoldal, 1989; Fischer *et al.*, 2014]. Biomass as high as 20 mg Chl *a*/m³ can be commonly observed [Kogeler and Rey, 1999; Wassmann *et al.*, 1999; Engelsen *et al.*, 2002]. The spring bloom is supported by large stocks of nutrients accumulated during the preceding winter [Rey, 2004] and peaks in May with a mean satellite derived Chl *a* > 2.0 mg/m³. Phytoplankton biomass significantly decreases in June (Chl *a* < 1.0 mg/m³) due to nutrient depletion and stronger zooplankton grazing [Wassmann *et al.*, 2006]. A summer bloom then develops in July–August dominated by coccolithophores, which are favored by a thin Mixed Layer (of about 20 m), warm surface waters, high PAR, and adapted to low nutrient levels. In late summer, the decrease in vertical stratification by surface cooling and wind mixing favors the supply of nutrients to the surface waters. Such nutrient

suggest that the volume of Atlantic Water has more than doubled (from $33 \times 10^3 \text{ km}^3$ to $84 \times 10^3 \text{ km}^3$) over the last 30 years. The volume of Arctic Water decreased by a factor of two, and the volume of the Barents Sea Water remained relatively unchanged [Oziel *et al.*, 2016]. These changes in the hydrographic characteristics of the Barents Sea were mainly associated with northwards shifts of both the Northern and Southern Fronts [Oziel *et al.*, 2016].

The Barents Sea is a highly productive shelf sea, connecting the Atlantic to the Arctic Ocean. Primary production represents approximately 40% of that attributed to the total Arctic shelves [Sakshaug, 2004; Ardyna *et al.*, 2013; Arrigo and van Dijken, 2015]. Intense phytoplankton blooms are reported every year, supported by elevated winter stocks of nutrients supplied by vertical mixing and advection of Atlantic Water, and benefit from a late phasing of zooplankton grazing

replenishment promotes late summer blooms if, in addition, the irradiance in the euphotic zone is high enough to sustain algal photosynthetic activity [Ardyna *et al.*, 2013, 2014].

In this study, we investigate how the recently changing physical environment impacts phytoplankton blooms in the Barents Sea. More specifically, we examine how the observed climate-driven hydrographic trends of increasing Atlantic Water volume, changing water masses, and shifting oceanic fronts previously identified by Oziel *et al.* [2016] affect the spatiotemporal distribution of calcifying and noncalcifying phytoplankton obtained from the last 17 years of ocean color data (1998–2014).

2. Materials and Methods

Our analyses are based on the hydrographic data set compiled by Oziel *et al.* [2016] including an in situ biogeochemical database (Chl *a* and nutrients), a general circulation model, and ocean color satellite derived products (Chl *a*, PAR, PIC, euphotic depth) covering the period 1998–2014. The study domain (black frame in Figure 1) extends from 10°E to 65°E and from 70°N to 80°N. It covers a larger area than the one considered by Signorini and McClain [2009] (15–50°E, 69°N–77°N) and includes the ice edge in April and May, allowing the ice edge phytoplankton bloom to be captured.

2.1. In Situ Data

The International Council for the exploration of the Sea (ICES, <http://ocean.ices.dk>) and the Arctic and Antarctic Research Institute (AARI) [Ivanov *et al.*, 1996; Korablev *et al.*, 2007] provided hydrographic data [Nilsen *et al.*, 2008] that have been merged in a new database [Oziel *et al.*, 2016]. This database contains more than 130,000 CTD profiles and thus stands out as one of the most complete hydrographic collections of the Barents Sea. This data set was used to locate oceanic fronts and define water masses based on temperature, salinity, and density criteria [Oziel *et al.*, 2016]. Briefly, Atlantic Water is characterized by salinity $S > 34.7$ and temperature $T > 3^{\circ}\text{C}$, with density anomalies σ generally larger than 27.6 kg/m^3 . Arctic Water has $S < 34.4$ and $T < 0^{\circ}\text{C}$, Barents Sea Water has $T < 3^{\circ}\text{C}$ and $S > 34.7$, with $\sigma > 27.8 \text{ kg/m}^3$, and the Norwegian Coastal Water has $S < 34.4$ and $T > 3^{\circ}\text{C}$.

The MLD was computed as the depth h for which the difference in potential density between depth h and the surface $\Delta\sigma(h) = \sigma(h) - \sigma_0$ first exceeds 0.1 kg/m^3 [Peralta-Ferriz and Woodgate, 2014]. We also determined the Brunt-Väisälä frequency N^2 , which characterizes the stability of the water column, from the approximate relation $N^2 = (g/\rho)(d\rho/dh)$ where $g = 9.8 \text{ m/s}^2$, ρ is the density and h is depth. A water column is considered stable if $N^2 > 0$, and neutral/unstable if $N^2 \approx 0$. Monthly maps of SST, σ_0 and MLD have been derived by optimal interpolation of in situ measurements on a regular grid of 0.5° longitude by 0.25° latitude.

Dissolved inorganic nutrients (nitrates, dissolved silicates, and phosphates) and Chl *a* (HPLC) were provided by the Institute of Marine Research in Bergen (IMR Norway). The data covers the 1980–2010 period with 6394 stations. Analytical methods are described in Wassmann *et al.* [1990, 1991].

2.2. Satellite Data

Sea ice concentration data were obtained from monthly composites provided by the National Snow and Ice Data Center for a grid resolution of $25 \text{ km} \times 25 \text{ km}$ (data set ID NSIDC-0051) [Cavalieri *et al.*, 1996]. The data set provides a consistent time series of sea ice concentrations obtained from brightness temperatures acquired by several passive microwave instruments (SMMR, SSM/I, SSMIS) and covers the period 1979–2014.

The GlobColour database (<http://hermes.acri.fr>) provides a continuous data set of ocean color satellite data products from the merging of four ocean color sensors: MEdium Resolution Imaging Spectrometer (MERIS), Moderate Resolution Imaging Spectroradiometer (MODIS), Sea-viewing Wide Field-of-view Sensor (SeaWiFS), and Visible Infrared Imaging Radiometer Suite (VIIRS). These sensors measure visible and near-infrared solar radiation emerging from the ocean surface layer. Such remotely sensed information is only available during the daytime and in the absence of ice and clouds. Under-ice phytoplankton and sea ice microalgae cannot be seen by ocean color remote sensing and are thus not included in this paper, though we are aware that these algae may substantially contribute to primary production [e.g., Gosselin *et al.*, 1997; Arrigo *et al.*, 2014].

Weekly and monthly data of ocean color satellite products including euphotic depth, PAR, Chl *a*, and PIC at 4.6 km spatial resolution were downloaded for the period 1998–2014. The GlobColour Chl *a* product for

case 1 waters (open ocean waters) is generated from the Garver-Siegel-Maritorena merging model which uses the normalized remote sensing reflectances at the original sensor wavebands [Maritorena *et al.*, 2010]. Ocean color Chl *a* products have already been used and validated in the Barents Sea [e.g., Mitchell *et al.*, 1991; Engelsen *et al.*, 2002; Qu *et al.*, 2006; Signorini and McClain, 2009; Dalpadado *et al.*, 2014]. Kogeler and Rey [1999] and Engelsen *et al.* [2002] have shown that satellite-derived Chl *a* correspond well with Chl *a* in the upper 40–50 m in the central Barents Sea. Here, the quality of the data set is reassessed by comparison with the Chl *a* in situ database (see supporting information Figure S1). Among 6394 stations, 566 matchups were found. The best matchups were observed when in situ Chl *a* were averaged over the first 20 m. The coefficient of determination r^2 between these corresponding sets of values (satellite and in situ) is equal to 0.4, the mean ratio is 0.79 and the standard deviation is 2.02. The slope of the regression line is equal to 0.80, which is close to the mean ratio. This figure shows the good correspondence between both types of data. The binning of the Chl *a* excludes pixels for which coccolithophores are detected by using reflectance thresholds independent from the PIC [Moore *et al.*, 2012]. This process thus excludes the estimation of Chl *a* in the presence of coccolithophore blooms even though coccolithophore cells contain a small amount of Chl *a* (<0.3 pg cell $^{-1}$) [Daniels *et al.*, 2014].

The GlobColour PIC product is a weighted average of three single-sensors (MODIS, SeaWiFS, and VIIRS) level 3 PIC products derived from NASA's standard PIC algorithm [Gordon *et al.*, 2001; Balch *et al.*, 2005]. The basis for this algorithm is a robust relationship between the light backscattering coefficient and the concentration of coccoliths, calcite plates forming the coccosphere of the coccolithophores [Balch *et al.*, 1991; Paasche, 2002]. Some coccolithophore species, including *Ehux*, overproduce and release excess coccoliths into the water during the later stages of a bloom [Borman *et al.*, 1983; Westbroek *et al.*, 1989; Feng *et al.*, 2008], creating large patches of highly reflective waters, which can be easily observed from space [e.g., Holligan *et al.*, 1993]. In the Barents Sea, satellite-derived PIC concentration provides a good proxy for *Ehux* coccolith concentration because *Ehux* dominate the coccolithophore population in the Barents Sea [Giraudeau *et al.*, 2016]. Moreover, satellite PIC products have been successfully validated during *Ehux* blooms in the Barents Sea [Hegseth and Sundfjord, 2008; Hovland *et al.*, 2014], as well as in the global ocean [Hopkins *et al.*, 2015].

2.3. Ocean Circulation Model

SINMOD (SINtef Ocean MODel) [Slagstad and Wassmann, 1996] is a three-dimensional ocean circulation model coupled with an ice model [Hibler, 1979] and a biogeochemical model with two phytoplankton groups. Atmospheric forcing is provided by reanalysis ECMWF (ERA interim). The model has been used in the area for over 25 years for biogeochemical purposes [e.g., Ellingsen *et al.*, 2008; Wassmann *et al.*, 2010; Reigstad *et al.*, 2011; Oziel *et al.*, 2016]. Here, we use SINMOD to: (1) identify the position of oceanic fronts and define domains occupied by Atlantic, Arctic, and Barents Sea Waters following the technique described and validated by Oziel *et al.* [2016] because hydrological observations are too sparse; (2) study the seasonal atmospheric forcings (winds and total heat fluxes).

3. Results

3.1. Biogeographical Phenology of Phytoplankton and Environmental Parameters

Phenology of Chl *a* and PIC for the period 1998–2014 averaged over the Barents Sea, and over the domains occupied by the Atlantic Water, the Barents Sea Water, and the Arctic Water are shown in Figure 2. We considered bloom thresholds of 0.8 mg Chl *a*/m 3 and 0.5 mmol PIC/m 3 derived by Hopkins *et al.* [2015]. From the climatology, the spring bloom peaked in May with Chl *a* concentration averaged over the entire Barents Sea of about 4 mg/m 3 . The spring bloom was more intense in Barents Sea Water than in Atlantic or Arctic Water, reaching a total of about 5 mg Chl *a*/m 3 . From July to August, Chl *a* remained low at 0.7 mg/m 3 but increased again in September reaching 1 mg Chl *a*/m 3 . From early spring until early summer (April–June), the average PIC over the entire Barents Sea remained below 0.05 mmol/m 3 . During the summer, Barents Sea averaged PIC concentrations increased up to about 1.4 mmol/m 3 in late July, thereby lagging behind the spring Chl *a* peak by about 3 months, which is consistent with seasonal trends observed by Signorini and McClain [2009]. Interestingly, the highest PIC reached was observed in the Atlantic Water (2.5 mmol/m 3 ; Figure 2). The temporal mismatch found between the summer peaks of PIC and Chl *a* in Figure 2 reinforce that these blooms are distinct.

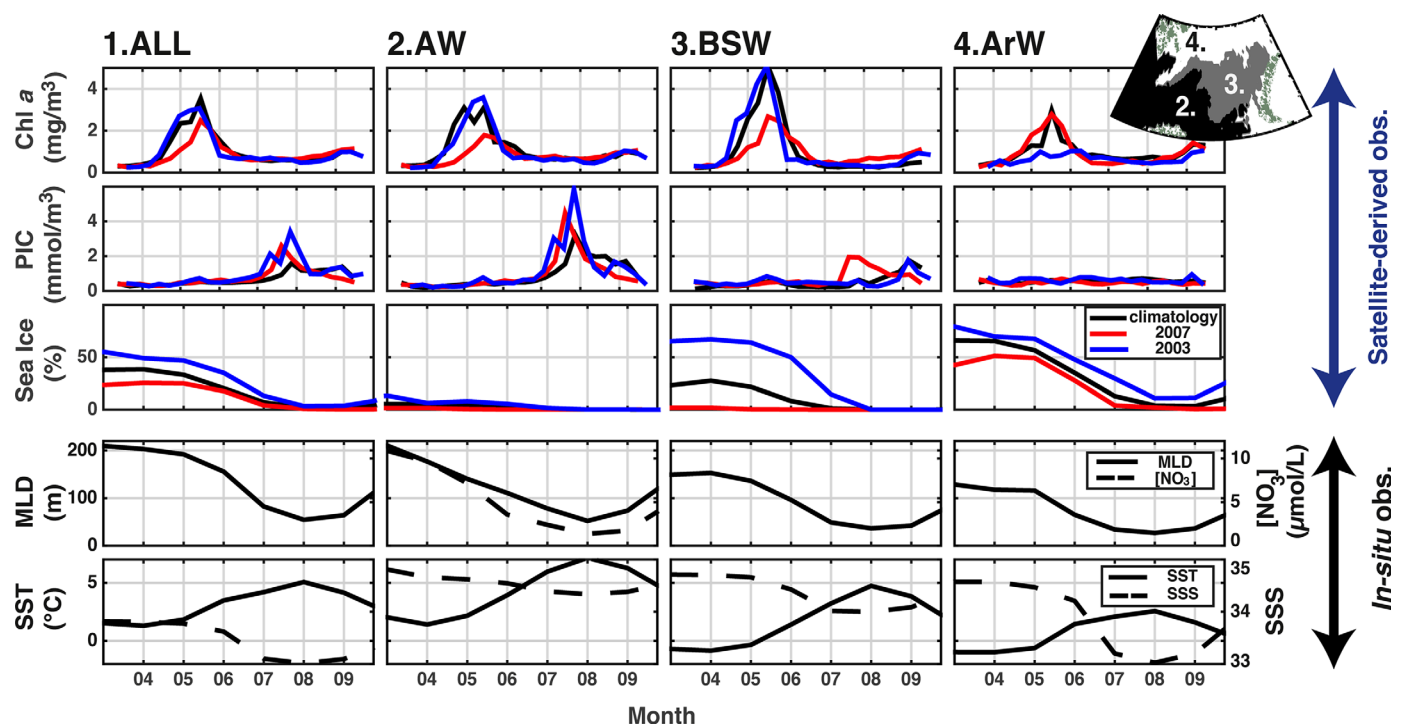


Figure 2. Seasonal cycles of satellite-derived data (Chl *a*, PIC, and sea ice concentration) and in situ hydrological parameters (MLD = Mixed Layer Depth; SST = in situ Sea Surface Temperature; SSS = in situ Sea Surface Salinity) for different areas (1 = Entire Barents Sea, 2 = Atlantic Water domain, 3 = Barents Sea Water domain, 4 = Arctic Water domain). In situ nitrate concentrations ($[\text{NO}_3]$) are averaged within the BSO section between 0 and 200 m. Satellite data show seasonal cycles for a cold year (2003), a warm year (2007), and a climatological year (1998–2014 average); in situ data only show the climatological seasonal cycle (1980–2012 average).

To support the existence of the second noncalcifying bloom, we exploited the large in situ Chl *a* database covering our study area (Figure 3). The late summer samples (from late July to early October) are indicated by gray dots; and those corresponding to a bloom (Chl *a* concentration averaged in the 0–50 m layer higher than the bloom threshold 0.8 mg/m^3) are indicated by red dots. The samples, corresponding to the observation of late summer noncalcifying blooms, account for 14.6% of the total number of summer samples and are mainly (84.8%) located in the Atlantic Water area. The in situ Chl *a* concentration database thus confirms the occurrence and large distribution of late summer blooms detected by remotely sensed data.

The seasonal cycle of environmental parameters associated with the onset and demise of phytoplankton blooms in the Barents Sea is also shown in Figure 2. These parameters include sea ice concentration, MLD, Sea Surface Temperature (SST), Sea Surface Salinity (SSS), and nitrate concentrations (averaged over the 0–200 m depth interval of the Barents Sea Opening, BSO, section in the southwestern Barents Sea shown in Figure 1). With the rise of incident PAR (supporting information Figure S2) from early April ($5 \text{ mol/m}^2/\text{day}$) to May ($35 \text{ mol/m}^2/\text{day}$), sea ice started to melt and SST rose, resulting in a decrease in SSS and therefore a shoaling of the MLD.

Phytoplankton starts growing when MLD decreases in April (Figure 2). At this time, the euphotic depth (Zeu, see Morel *et al.* [2007]) is about 50 m (supporting information Figure S2). In order to meet optimal conditions for the spring bloom, the MLD theoretically needs to reach about the same depth to avoid transportation of the phytoplankton out of the euphotic layer [Sverdrup, 1953, updated by Fischer *et al.*, 2014]. The largest SST increase took place in the Atlantic Water area (from 2°C in March to 8°C in August) whereas the largest SSS decrease occurred in the Arctic Water area (from 34.6 to 33). The shallowest MLD found in May in the Arctic Water area (100 m on average versus 140 m in the Atlantic and Barents Sea Water areas) showed that ice-melt induced haline stratification in the North is more efficient than the thermal stratification in the South but does not validate the Sverdrup theory for the Barents Sea. The nutrient concentrations (i.e., nitrates) then decreased from the winter maximum ($[\text{NO}_3] = 10\text{--}12 \text{ }\mu\text{mol/L}$, $[\text{SiO}_2] = 4\text{--}6 \text{ }\mu\text{mol/L}$, $[\text{PO}_4] = 0.6\text{--}0.8 \text{ }\mu\text{mol/L}$) and followed the seasonal evolution of the MLD at the Barents Sea Opening. These were almost consumed to depletion by the end of July ($[\text{NO}_3] \approx 1.5 \text{ }\mu\text{mol/L}$, $[\text{SiO}_2] \approx 1.5 \text{ }\mu\text{mol/L}$, and $[\text{PO}_4]$

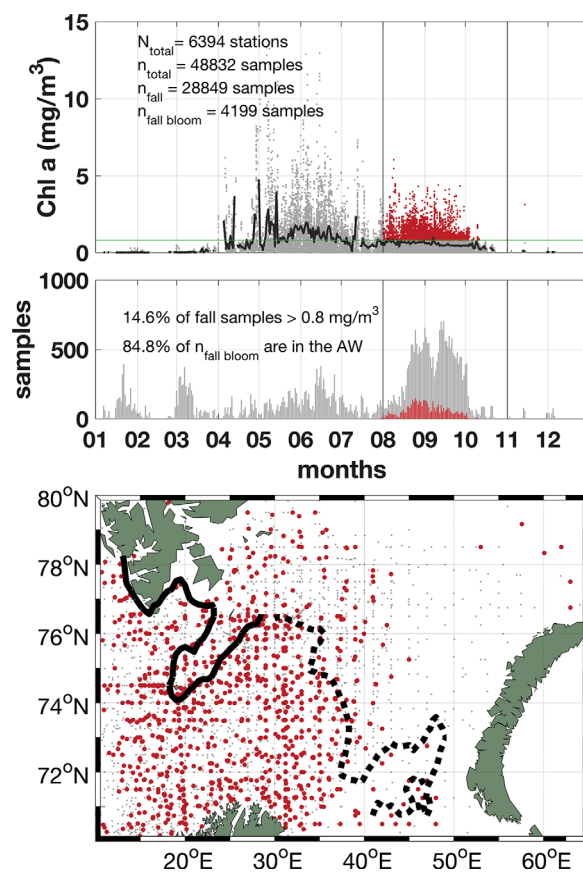


Figure 3. (top) Seasonal distribution of all in situ Chl *a* samples in gray, Chl *a* samples corresponding to late summer blooms in red, and daily averaged Chl *a* in dark solid line. (middle) Seasonal samples count histogram, red bars account for samples corresponding to fall blooms. (bottom) Location of all stations in grey and stations that correspond to a fall bloom in red. The solid line shows the Polar Front, the dotted line the Southern Front.

Our climatological analysis of the physical and biological environment revealed overall seasonal patterns in the Barents Sea. The next section investigates the interannual variability and the trends over the 1998–2014 period. From the 17 year time-series, two distinct climatic years were clearly distinguished by contrasted sea ice extent as well as physical and biological environments.

3.2. Interannual Variability and Trends Over the Period 1998–2014

The interannual variability of environmental parameters as well as Chl *a* and PIC concentrations were examined over the ocean color remote sensing period, 1998–2014. The winter sea ice extent decreased by about 35% over the last 30 years (Figure 5a). The mean MLD averaged over the entire study area in August–September increased by about 15 cm/yr over the period 1980–2012 (Figure 5b). A decreasing trend in stratification, $\Delta\sigma$, (difference between the surface density and the density at 100m) of about 0.015 kg/m³/yr was observed in summer (Figure 5c). However, increased summer mixing is not paralleled by increased nutrient stocks in winter, and therefore did not necessarily imply increased nutrients in summer available for phytoplankton. The mean nitrate concentration at the BSO section in winter decreased by about $-0.7 \mu\text{mol/L/yr}$ (Figure 5d). Last, the annual mean concentration of Chl *a* and PIC over the entire study area normalized by the number of available pixels for each year, increased by about 110% and 50%, respectively (Figures 5e and 5f) between 1998 and 2014. In order to identify trends and contrasts in the interannual variability of the physical and biological environment, we used sea ice, which is a good indicator of Ocean-Air temperature variations [Oziel *et al.*, 2016], as a proxy.

$\approx 0.25 \mu\text{mol/L}$). At that time, when a coccolithophore bloom was observed, the MLD was minimal in the Atlantic Water (<50m) and SST was maximal ($\approx 8^\circ\text{C}$). In August, the stability of the water column weakened, the MLD deepened to reach $\approx 70 \text{ m}$ by mid-September, and a small summer bloom of noncalcifying phytoplankton developed.

The spatial distribution of the spring (May) Chl *a* climatology is shown in Figure 4a. High phytoplankton concentrations ($\geq 0.8 \text{ mg Chl } a/\text{m}^3$) were observed throughout the study area except west of 20°E and north of the Polar and Northern Fronts. In the northeastern Barents Sea (north of the Polar Front), very high Chl *a* concentrations ($>5 \text{ mg Chl } a/\text{m}^3$) were however found along the current flowing towards the Kara Sea. The Chl *a* September climatology depicted in Figure 4c indicates low concentration ($<0.8 \text{ mg/m}^3$) north of the Polar and Southern Fronts. Southward, Chl *a* averages 1–2 mg/m^3 (Figure 4c). As for calcifying phytoplankton, the PIC summer climatology (July–August) (Figure 4b) indicates highest concentrations south of the Southern Front, i.e., $>5 \text{ mmol/m}^3$ around 74°N – 35°E and remained below 0.3 mmol/m^3 in the rest of the study area. In summer, high biomass of both calcifying and noncalcifying phytoplankton blooms is shown by white contours in Figure 4. The blooms were well-confined to Atlantic Water delineated by the Polar and Southern Fronts.

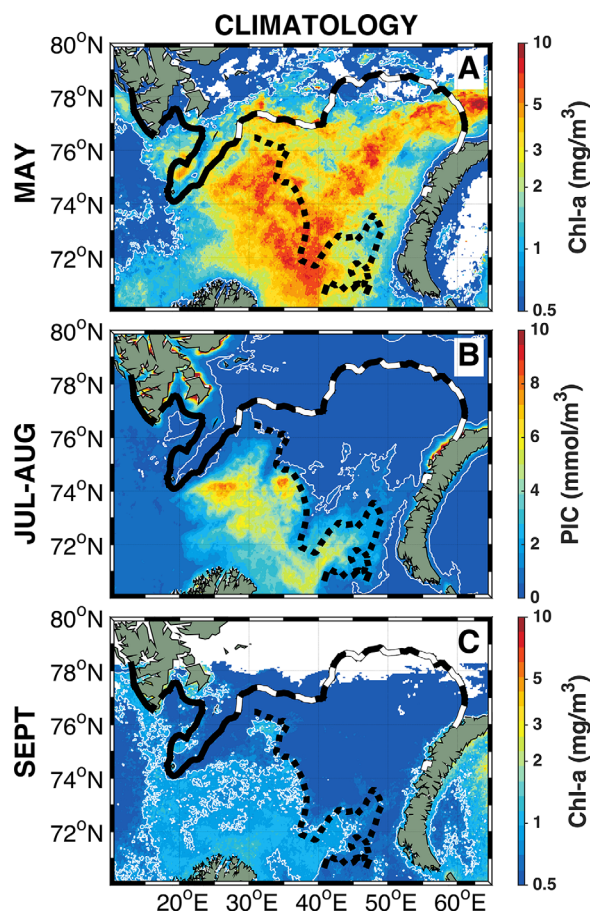


Figure 4. Climatologies of (a) Chl *a* in May (b) PIC in July–August, and (c) Chl *a* in September, over the period 1998–2014. The solid line shows the Polar Front, the dotted line the Southern Front, the dashed line the Northern Front, and the white thin contours delineate the bloom area.

meridional case (≈ 0.007) highlighting the fact that the shift is greater toward the East than towards the North.

Secondly, in order to characterize the year-to-year variability, we labeled years based on winter anomalies of the detrended sea ice extent. We used two different criteria. First, winter sea ice extent anomalies were calculated as deviations from the linear trend over the period 1997–2014 (Figure 5a). A threshold value of 50,000 km² in sea ice extent anomaly was chosen, which corresponds to roughly half of the standard deviation of the mean winter sea ice extent in 1997–2015. This allowed grouping the multiyear data set into ICE+ years (1998, 2003, 2004, 2010, and 2014; blue dots), ICE− years (2000, 2006, 2007, 2008, and 2012; red dots) and ICE= years (2001, 2002, 2005, 2009, 2011, 2013) (Figure 5a). Second, years with winter sea ice extent anomalies further than one standard deviation from the entire 1980–2014 period linear trend were selected, resulting in a set of ICE++ (1998, 2003, and 2004) and ICE−− years (2007 and 2012). Spring Chl *a* and summer PIC composites for ICE− and ICE+ data sets are shown in Figure 7 (the ICE−− and ICE++ data sets are in supporting information Figure S3).

The spring Chl *a* composite maps for ICE− (Figure 7c) and ICE−− (supporting information Figure S3) show similar patterns: two distinct phytoplankton bloom areas, one near the ice edge and the other in the open sea, separated by an area of low phytoplankton biomass around 75°N. This feature was more pronounced in the ICE−− composite because the criterion used was more severe (i.e., largest sea ice extent anomalies). In contrast, during ICE+ years (Figure 7a; ICE++, supporting information Figure S3), phytoplankton biomass was more uniformly spread over the Barents Sea and the position of the ice edge extended further south than in ICE− years. The phytoplankton bloom area during ICE+ years appears to be the superposition

First, to detect trends in the spatial distribution of the blooms, we computed the averaged biomass proxy concentrations ([Chl *a*] and [PIC]) in a northern area ($>74^\circ\text{N}$), a southern area ($<74^\circ\text{N}$), an eastern area ($>40^\circ\text{E}$), and a western area ($<40^\circ\text{E}$). Meridional (zonal) ratios were obtained by dividing the averaged values of the North (East) by those of the South (West). These ratios allow us to characterize the meridional and zonal phytoplankton bloom distributions, respectively. Large (small) ratios >1 (<1) indicate that the biomass is located in the North (South) or East (West). We then compared sea ice concentration anomalies with these ratios each year (see Figure 6). Negative linear relationships between the increasing sea ice concentration anomalies and the ratios provide evidence for a northerly and easterly shift of the phytoplankton blooms as sea ice declines. For spring and late summer Chl *a* blooms, strong and significant linear relationships between sea ice anomalies and meridional/zonal ratios are characterized by large coefficients of determination, r^2 , equal to 0.64/0.80 and 0.62/0.73, respectively. This relationship is not as clear for the early summer calcifying bloom ($r^2 = 0.02/0.32$) and primarily shows an eastward shift (the northward shift is not significant, p -value = 0.55). Finally, mean slopes of the linear trends of these ratios show for all blooms larger values for the zonal case (≈ 0.033) than for the meridional case (≈ 0.007) highlighting the fact that the shift is greater toward the East than towards the North.

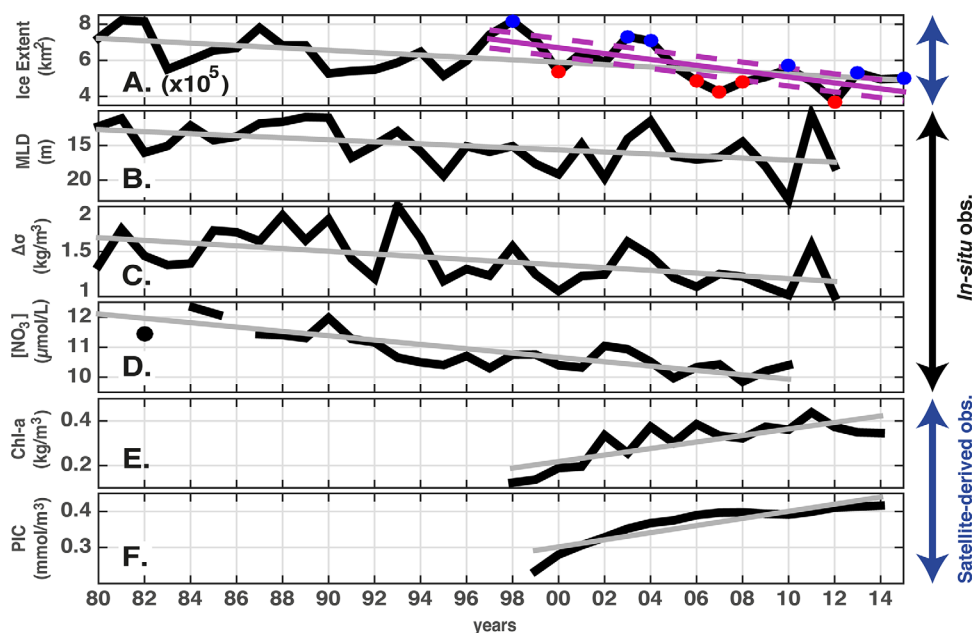


Figure 5. Time series of (a) winter maximal Sea Ice extent, (b) summer Mixed Layer Depth, MLD, (c) stratification, $\Delta\sigma$ ($\sigma_{\theta} - \sigma_{100m}$), (d) winter (January–March) nitrate concentration at the BSO section integrated over the depth interval 0–200 m, (e) annual mean satellite Chl *a*, and (f) annual mean satellite Particulate Inorganic Carbon, PIC. Data in Figures 5e and 5f are normalized by the amount of available pixels. Lines denote trend over their temporal domain. Magenta-dashed lines correspond to a deviation of $\pm 50,000$ km² from the trend line shown in magenta. PIC value in 1998 is missing. Nitrate values for 1980, 1983, and 1986 are missing.

of the ice-edge and open sea phytoplankton blooms retrieved for ICE– years (Figure 7c). The contrast in spatial distribution of phytoplankton biomass between ICE+ and ICE– during the summer PIC and Chl *a* blooms was also striking. During ICE– years (Figures 7f and 7i and ICE–, supporting information Figure S3), the bulk of coccolithophore and noncalcifying biomass was mainly located east of 35°E, up to the Southern Front. By contrast, during ICE+ years, the bulk of coccolithophore and noncalcifying phytoplankton biomass was mainly found west of 35°E and did not reach all the way up to the Southern Front (Figures 7d and 7g). The transition between the ICE+ and the ICE– years is illustrated by the ICE= composites (Figures 7b, 7e, and 7h).

The Barents Sea biogeochemical environment has experienced major changes during the last 30 years. Sea ice extent appears to be a major factor determining the spatial distribution of phytoplankton blooms in the Barents Sea not only over the long-term but also on a the year-to-year time scale. The observed changes in the other environmental factors such as mixing/stratification mechanisms in the open sea and the import of new nutrients could also be important. To improve our understanding about the mechanisms that drive the spatial and inter-annual variability, we investigated the physical environment and phytoplankton distribution in a year of minimum (2007) and a year maximum (2003) sea ice extent. These two contrasting years were selected on the basis of sea ice extent anomalies (Figure 5a) and the availability of hydrological and biogeochemical data sets.

3.3. Spatiotemporal Variability of Phytoplankton and Water Masses: Comparison Between A Year of Maximum (2003) and Minimum (2007) Sea Ice Extent

The winter maximum sea ice extent of 2007 was the second lowest on record and was about twice as low as that of 2003 (50% of sea ice coverage, Figure 2). The southernmost latitude reached by the ice edge in the eastern Barents Sea remained above 77°N in 2007 whereas the ice edge roughly followed the 74°N parallel in 2003 (red line in Figure 8).

3.3.1. Remotely Sensed Phytoplankton Biomass

The characteristics of the spring bloom in 2003 resembled those of a climatological year in Atlantic and Barents Sea Waters, but not in Arctic Water where Chl *a* remained below 1 mg/m³ throughout the year (Figures 2 and 8). In 2007, the spring bloom peaked in mid-May as in the climatological and 2003 years but its growth was slower (lower slopes in Chl *a* throughout spring; Figure 2, red line) and a smaller biomass was reached in both the Atlantic Water and Barents Sea Water areas but not in Arctic Water (Figure 2, red line).

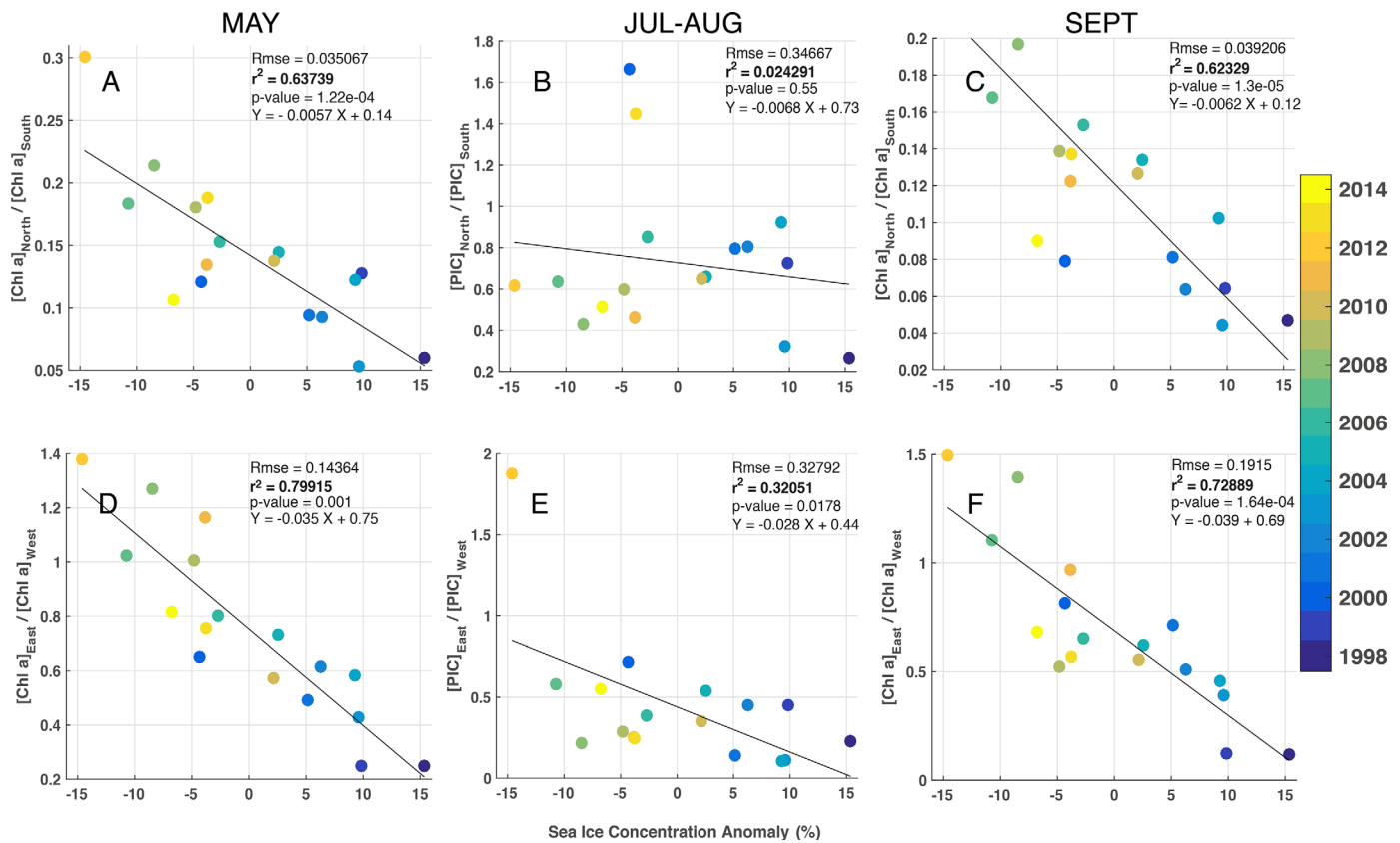


Figure 6. Relationship (coefficient of determination r^2 , Root Mean Square Error $Rmse$, p -values, and slopes of the linear-type II regression) among sea ice concentration anomalies and: $[Chl\ a]_{North} / [Chl\ a]_{South}$ ratios for May (a), and September (c); $[Chl\ a]_{East} / [Chl\ a]_{West}$ ratios for May (d), and September (f); $[PIC]_{North} / [PIC]_{South}$ ratios for July–August (b); and $[PIC]_{East} / [PIC]_{West}$ ratios for July–August (e).

The Chl a maximum reached in Atlantic Water and Barents Sea Water were roughly twice smaller than those corresponding to the climatology and the 2003 year (Figure 2).

Biomass concentrations higher than $1\text{ mg Chl } a / \text{m}^3$ were exclusively found along the ice edge and the Southern Front in April for both years (Figures 8a and 8b). At the peak of the spring bloom (May), 2003 and 2007 Chl a concentrations were similar to those of the composites, respectively ICE+ and ICE-. In 2007, Chl a concentrations higher than 10 mg/m^3 were observed in two distinct regions, one along the ice edge, and the other south of 74°N . Indeed, due to the extreme northward position of the ice edge, the ice-edge spring bloom was geographically separated from the spring bloom in the Atlantic Water and the Coastal Water (Figure 8d). In May 2003, Chl a concentrations in the ice-free area generally exceeded 3 mg/m^3 with some maximums at 30 mg/m^3 (Figure 8c). The geographical separation between the ice-edge and the open water bloom identified in 2007 no longer exists. Interestingly, the retrieved Chl a in spring are twice as high as in 2007 when averaged over the entire Barents Sea area, the Atlantic Water area, or the Barents Sea Water area (Figure 2) suggesting that the ice-edge and open water blooms were superimposed. By June, at the end of the spring bloom, phytoplankton concentration dropped below 1 mg/m^3 in these regions except along the Polar and Northern Fronts in 2007 (Figure 8f).

A summer coccolithophore bloom began in June and culminated at the end of July with PIC concentrations of about 4 mmol/m^3 in 2003 when averaged over the entire Barents Sea area (versus 3 mmol/m^3 in 2007) and about 5 mmol/m^3 in the Atlantic Water (versus 4 mmol/m^3 in 2007), values both higher than those obtained during a climatological year (Figure 2). The spatial distribution of PIC shows that the coccolithophore bloom was mainly confined to the Atlantic Water, where concentrations of PIC up to 10 mmol/m^3 were reached over a large area (Figure 9). In 2007, the PIC distribution followed the Polar and Southern Fronts. In 2003, the coccolithophore bloom was situated more westward and southward, at $22^\circ\text{E}–34^\circ\text{E}$, $71^\circ\text{N}–73^\circ\text{N}$.

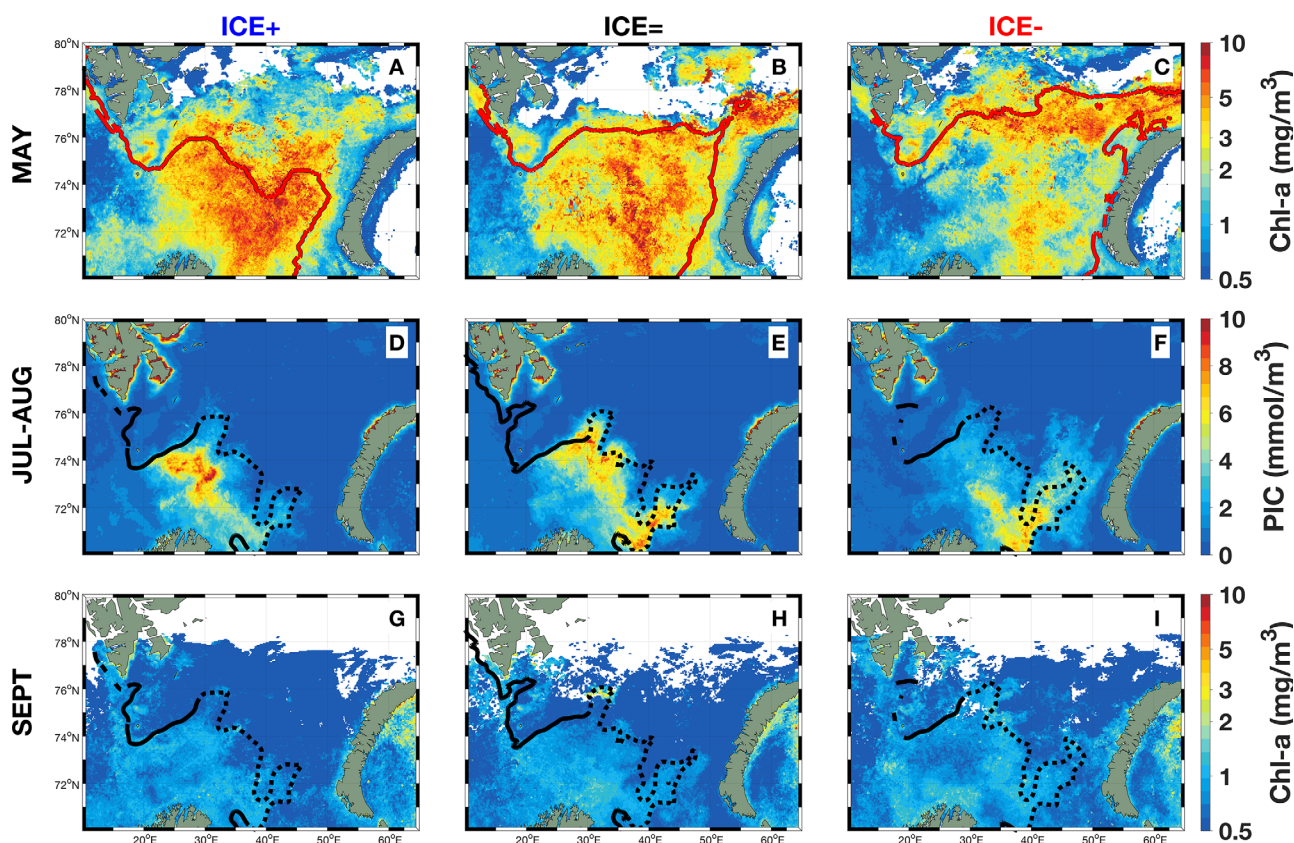


Figure 7. Maps of composites of satellite Chl *a* in May and September, PIC in July–August for ICE– years, ICE= years, and for ICE+ years. The red line denotes the ice edge corresponding to the 15% sea ice concentration isoline. Solid black line is the Polar Front, dotted line is the Southern Front.

A late-summer bloom of noncalcifying phytoplankton followed 1 month later in the Atlantic Water for both years (in late August or early September, Figure 2). Moderate concentrations of Chl *a* ($>1 \text{ mg/m}^3$) were mainly found in the Atlantic Water area with approximately the same spatial distribution as the earlier coccolithophore bloom (Figures 8i and 8j).

3.3.2. In Situ Physical and Biogeochemical Data

Environmental factors controlling phytoplankton blooms were analyzed using in situ physical and biogeochemical parameters measured along the Vardø cross section (Figure 1) in March, July, and September 2007 (Figure 10) and in September 2003 (Figure 11). This section runs from 72°N to 77°N along the 31°E meridian and sampled Norwegian Coastal Water, Atlantic, Arctic, and Barents Sea Waters (Figure 1). Unfortunately, no data are available for May 2007, thereby preventing an analysis during the spring bloom along the section. However, May data are available for the next year of minimum sea ice extent, 2008, along a small section north of Vardø across the ice edge (Figure 10b), providing a means to analyze the ice-edge bloom in a year of low sea ice extent. Data is only available for September in 2003.

Measurements of Chl *a* were also made along this section and provide insights into the vertical phytoplankton distribution, which is not accessible from ocean color remote sensing. In situ measurements of PIC are not available, thus impeding differentiation between calcifying and noncalcifying phytoplankton.

In winter (March), atmospheric (heat losses and strong winds, supporting information Figure S4) and ice conditions (Figure 2) over the Barents Sea ensure a strong mixing over the entire water column. Before the onset of the spring bloom, the water column was homogeneous ($N^2 \approx 0$, Figure 10a). Nitrate concentrations were abundant ($>6 \mu\text{mol/L}$) throughout the section and were maximal ($11 \mu\text{mol/L}$) where the Atlantic Water meets the denser Barents Sea Water formed in winter (73.5°N – 75°N).

In May, Figure 10b, melt water progressively mixed with surface water, creating an upper layer of lighter water. Heating and melting stabilized a shallow MLD ($\approx 20 \text{ m}$) where high phytoplankton biomass was

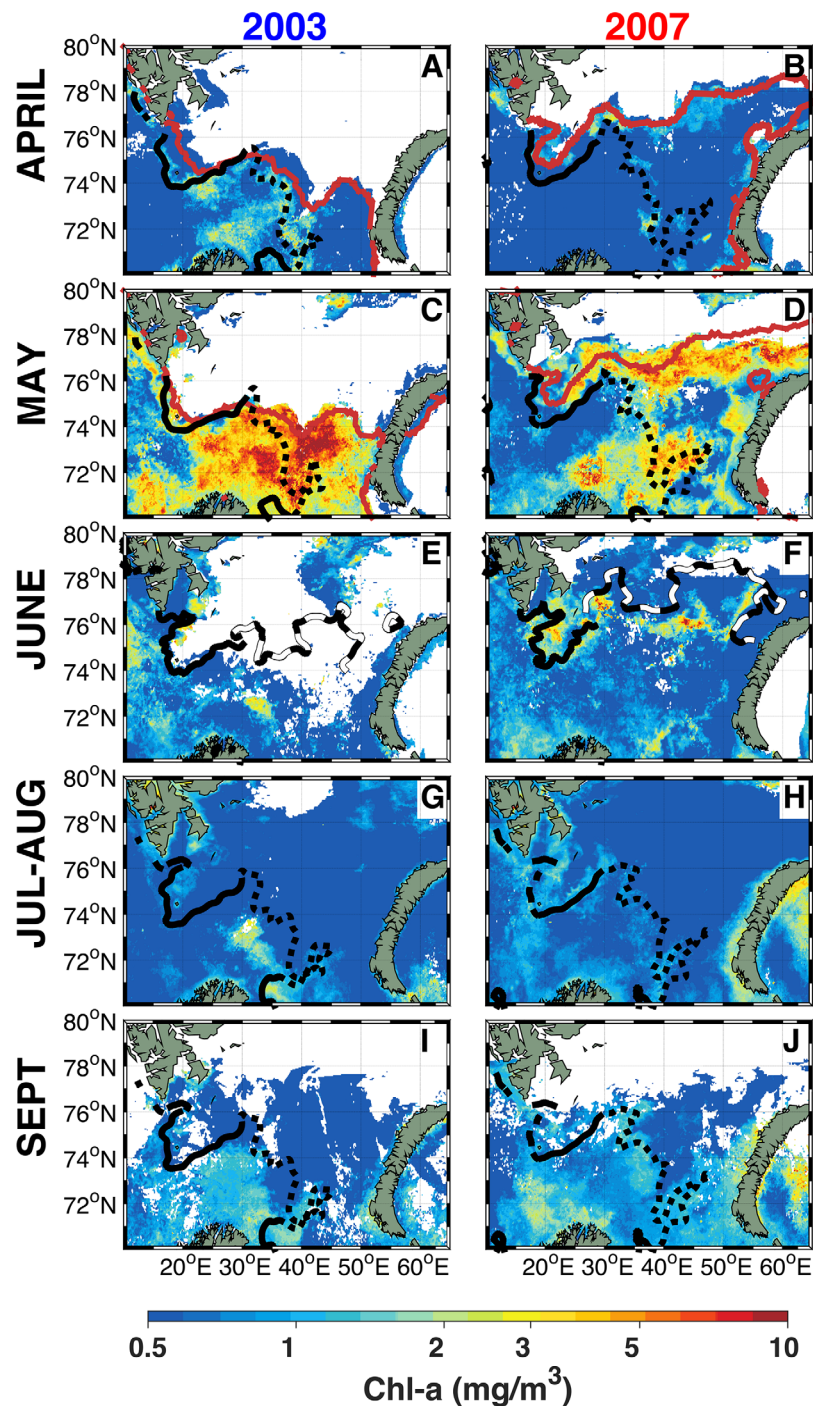


Figure 8. Maps of satellite Chl *a* averaged for the months of April, May, June, July–August, and September 2003 and 2007. The red line denotes the sea ice edge corresponding to the 15% sea ice concentration isoline in March. Solid line is the Polar Front, dotted line is the Southern Front, and dashed line is the Northern Front.

reached ($\text{Chl } a \approx 12 \text{ mg/m}^3$). Elsewhere, the stratification remained moderate, with an upper MLD generally deeper than 70 m (Figure 2) and relatively low Chl *a* concentrations ($0.5\text{--}3 \text{ mg/m}^3$).

Observations along the Vardø cross section in July were generally representative of a postbloom situation (Figure 10c). Surface water nutrients had been depleted ($[\text{NO}_3] < 1 \mu\text{mol/L}$) and phytoplankton biomass was very low ($\text{Chl } a \approx 0.3 \text{ mg/m}^3$). Phytoplankton was found at or slightly above the euphotic depth where nutrient concentrations were sufficient ($[\text{NO}_3] \approx 2\text{--}4 \mu\text{mol/L}$) to sustain growth. At both ends of the section,

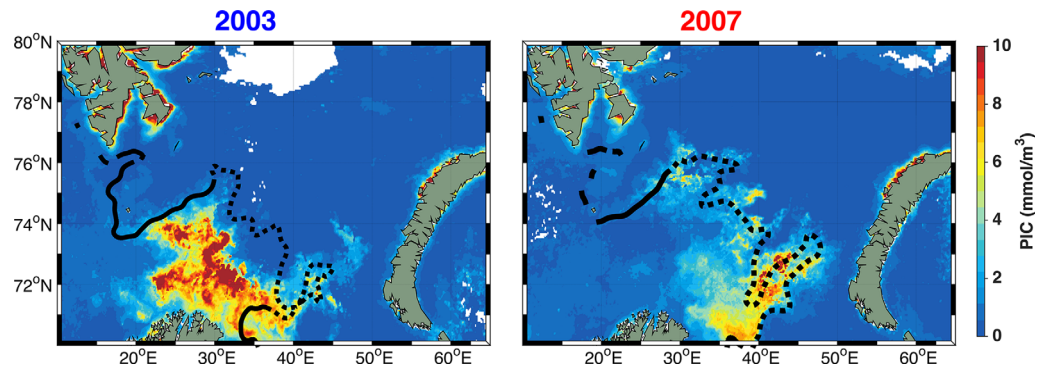


Figure 9. Maps of satellite PIC averaged for July–August 2003 and 2007. Solid line is the Polar Front and dotted line is the Southern Front.

at 70°–72°N and 76°–77°N, significant coccolithophore biomass was, however, found in near-surface waters, which is in good agreement with satellite-derived Chl *a* and PIC (Figures 8h and 9). The northern end is situated close to the Southern Front, where Atlantic Water shoaled over denser Barents Sea Water. This frontal structure is a place where potential vertical mixing is more likely as evidenced by the low values of the Brunt-Väisälä frequency (N^2) (Figure 10c). Vertical mixing along the Southern Front is collocated with a deepening of the 4 $\mu\text{mol/L}$ nitrate isoline (nitracline) down to 80m. The other high surface Chl *a* along the transect is situated in the Norwegian Coastal Water, which receives substantial nutrient input from freshwater run-off throughout the spring and summer. This nutrient-rich fresh Coastal Water invaded the surface layer up to 73°N and sustained phytoplankton development in these waters in July and September (Figures 10c and 10d).

The surface Chl *a* data along the Vardø section in September 2003 (Figure 11) and 2007 (Figure 10d) suggest a late summer noncalcifying phytoplankton bloom of moderate intensity, Chl *a* $\approx 0.7 \text{ mg/m}^3$, in the Atlantic Water (AW, red contours in Figures 10d and 11 top plots), a high phytoplankton biomass (Chl *a* $> 2 \text{ mg/m}^3$) in Coastal Water (CW, green contours), and a low phytoplankton biomass in melt water (Chl *a* $< 0.5 \text{ mg/m}^3$, surface water in blue contour).

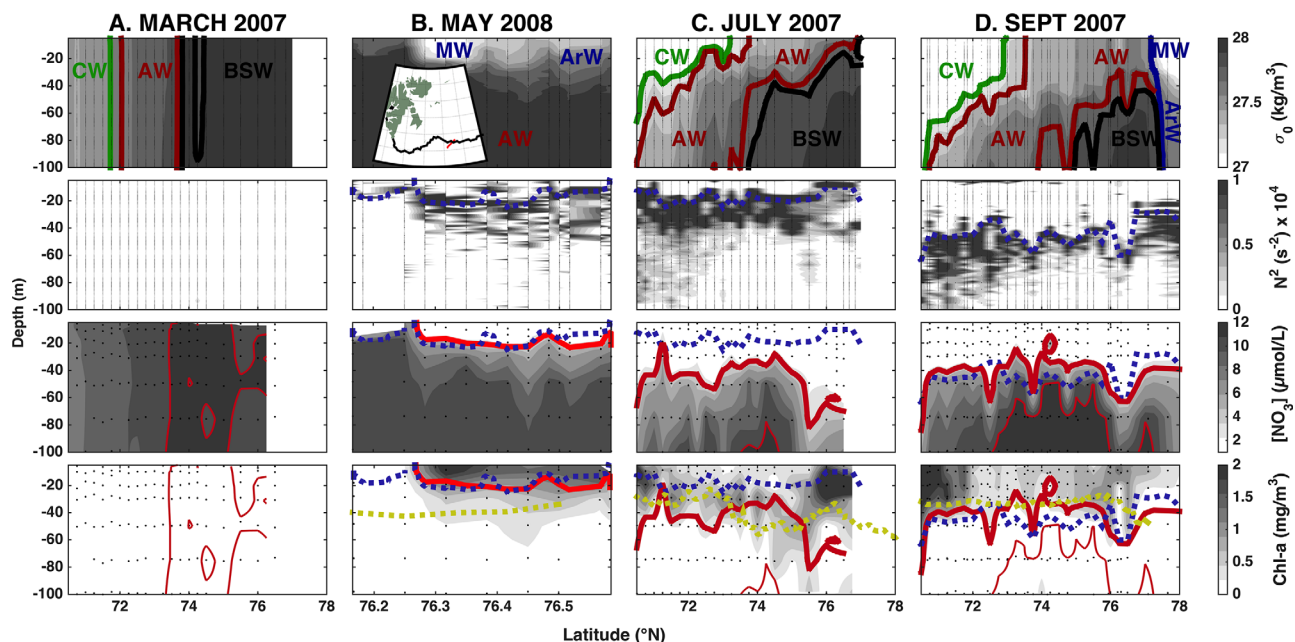


Figure 10. Hydrological and biogeochemical data along the Vardø section in (a) March 2007, (b) May 2008, (c) July 2007, and (d) September 2007. Potential density anomaly (σ_0) with water masses: CW = Coastal Water in green, AW = Atlantic Water in red, BSW = Barents Sea Water in black, ArW = Arctic Water in blue, MW = Melt Water in blue. Brunt-Väisälä frequency (N^2), Nitrate concentration, and Chl *a* concentration. Blue-dashed line = MLD, red thick and thin lines = 4 and 11 $\mu\text{mol/L}$ nitrate isolines, respectively, yellow-dashed line = Euphotic depth. Black dots represent sampling depths. Inset: map showing the section (red line) and the ice edge (black line) in May 2008.

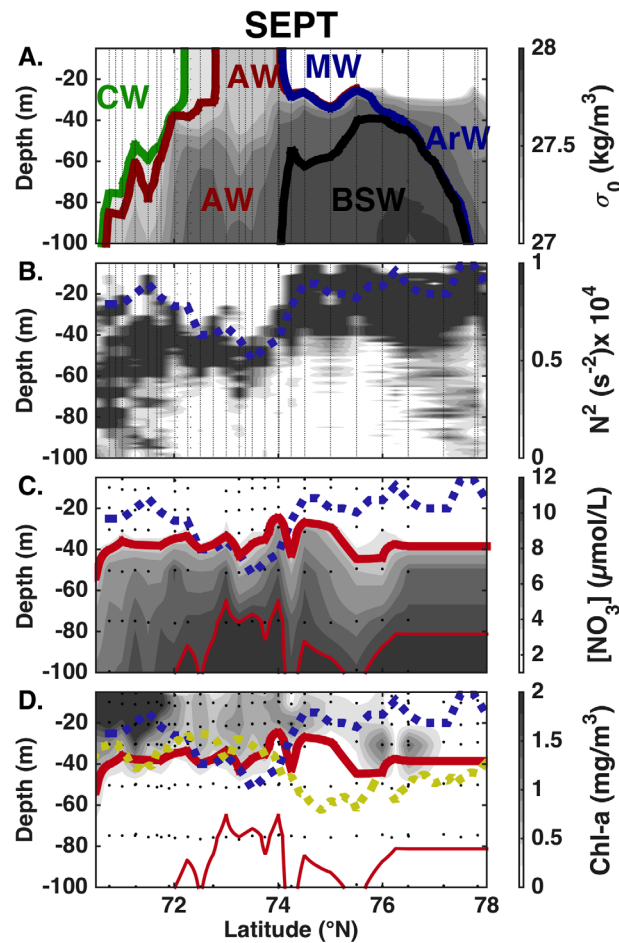


Figure 11. Hydrological and biogeochemical data along the Vardø section in September 2003. (a) Potential density anomaly (σ_0), (b) Brunt-Väisälä frequency (N^2), with water masses: CW = Coastal Water in green, AW = Atlantic Water in red, BSW = Barents Sea Water in black, ArW = Arctic Water in blue, MW = Melt Water in blue. (c) Nitrate concentration and (d) Chl-*a* concentration. Blue-dashed line = MLD, red thick and thin lines = 4 and 11 $\mu\text{mol/L}$ nitrate isolines, respectively, yellow-dashed line = Euphotic depth. Explain the dots.

to achieve this, we combined the hydrographic database of *Oziel et al.* [2016], biogeochemical (nutrients and Chl *a*) observations along transects and remotely sensed Chl *a* and PIC in the Barents Sea. The use of both remotely sensed Chl *a* and PIC (1998–2014) distinctly document the phenology of noncalcifying and calcifying phytoplankton. Three phytoplankton blooms were clearly detected throughout the Barents Sea: two blooms (May and September) mostly attributed to noncalcifying phytoplankton with in between a summer bloom composed of coccolithophores (late July). This study provides insights on how phytoplankton features (distribution, phenology, and magnitude) may respond to the environmental change of ongoing “Atlantification” of the Barents Sea.

4.1. Long-Term Trends and Interannual Variability in the Barents Sea

Over the last 30 years, the Barents Sea has experienced a drastic reduction in winter sea ice cover, doubling of the Atlantic Water volume, north-eastward shift of the fronts [*Oziel et al.*, 2016], decreased nitrate concentrations and, last, MLD deepening. In agreement, *Peralta-Ferriz and Woodgate* [2014] also found a deepening trend of the MLD in the southwestern part of the Barents Sea over the same period, although it was much stronger (+50 cm/yr). We suggest that the deepening of the MLD may be a consequence of both the decrease of winter sea ice extent (Figure 5a) that induces reduced melt water volume and the increased advection of Atlantic Water. At the Barents Sea entrance (BSO), the clear decrease in nitrates seems to be mainly related to processes occurring outside the Barents Sea, likely in the Nordic Seas. These upstream

In September, the deepening of the MLD below the 4 $\mu\text{mol/L}$ nitrate isoline and the creation of an unstable water column (Brunt-Väisälä frequency $N^2 \approx 0$) in the upper 50 m were observed. Such mixing is concomitant with a cooling of the atmosphere (the heat flux turns negative) and increasing winds, which occurred in late August in 2007 and about 1 month later in 2003 (supporting information Figure S4), thereby providing nutrients to phytoplankton in the surface layer (Figure 11c).

In contrast to 2007 observations, near-surface waters north of 74°N in 2003 were characterized by a density anomaly smaller than 27.2 kg/m^3 (Figure 11a). These low values suggest that this water was obtained from a mixing of nutrient-poor surface Arctic Water with melt water, resulting in low Chl *a* values. Higher Chl *a* values were found, at about 30 m depth, close to the 4 $\mu\text{mol/L}$ nitrate isoline (Figures 11c and 11d). This subsurface Chl *a* maximum is not detected by remote sensing (Figures 8i and 9) illustrating the complementarity between remote sensing and in situ data.

4. Discussion

This study is the first attempt to link over a 17 year period, the interannual variability of phytoplankton blooms with water mass distribution, oceanic fronts, and sea ice extent over the entire Barents Sea. To

processes could either be phytoplankton nutrient consumption, more stable stratification by surface freshening [Blindheim *et al.*, 1999] or thermal heating [Slagstad *et al.*, 2015], which could strengthen the halocline and decrease mixing with the nutrient-rich deeper layers. Such reductions in Barents Sea nutrient stocks are supported by modeling studies [Slagstad *et al.*, 2015] and in situ data, particularly for silicates, which are experiencing a much larger decrease than the nitrates [Rey, 2012]. Thus the “Atlantification” of the Barents Sea does not necessarily increase the advection of more nutrients from the North Atlantic.

Over the last 16–17 years, annual average Chl *a* and PIC concentrations increased significantly by about 100% and 50%, respectively. These positive trends were particularly marked in the northern and eastern Barents Sea, where changing sea ice conditions are critical. In agreement, a 30% increase of primary production trend was estimated by several other remote-derived studies [Bélanger *et al.*, 2013; Arrigo and van Dijken, 2015]. The observed increase in Chl *a* and primary production has been mainly attributed to a longer productive season, an increase in available light and an increase in the productive area [Arrigo *et al.*, 2008; Stroeve *et al.*, 2014]. Throughout the 17 year time-series, the spring phytoplankton bloom is by far the most prominent annual biological event, representing about 40–60% of the total annual Chl *a*, similar to observations for the Arctic Ocean as a whole [Ardyna *et al.*, 2013]. However, care must be taken when evaluating these trends considering that remote sensing data are limited to the surface of the open ocean. After the spring bloom, in situ data revealed that a SCM is created during a year of high sea ice extent. In addition, we know that phytoplankton blooms can occur beneath the sea ice [e.g., Mundy *et al.*, 2009; Arrigo *et al.*, 2012, 2014; Assmy *et al.*, 2017].

Interannual variability of Chl *a* in the Barents Sea is about 60%, in close agreement with the $75.2 \pm 10\%$ interannual variability of primary production obtained by numerical biogeochemical simulations in the European Arctic Corridor [Wassmann *et al.*, 2010]. This large interannual variability in primary production was mainly linked to large variability in the Air-Ice-Ocean physics. Using sea ice extent deviation from trend as a proxy, we highlighted two distinct climatic year types (i.e., ICE+ versus ICE– years). The relevance of these anomalous years is also largely supported by (1) temperature time series [i.e., Furevik, 2001; Oziel *et al.*, 2016], (2) the evidence of the North Atlantic Oscillation (NAO) influence on the Barents Sea [e.g., Loeng and Drinkwater, 2007] and (3) shifts in the whole Air-Ice-Ocean system [Smedsrud *et al.*, 2013]. Similar multiyears anomalies have been also detected in the Pacific sector [Overland *et al.*, 2012]. In the Barents Sea, they affect the spatial distribution of phytoplankton blooms (north-eastward shift) rather than their magnitude.

4.2. Environmental Factors Controlling the Spring Chl *a*: ICE– Versus ICE+ Years

We showed that the onset of blooms in spring was triggered by the stabilization of the water column in combination with large nutrient stocks built up during winter. Two distinct stratification mechanisms were identified: (i) heating in the southern and central ice-free Barents Sea and (ii) sea ice melting along the ice edge in the Seasonal Ice Zone (SIZ). During ICE+ years, these two processes overlap and allow a large build-up of Chl *a* in the spring over the entire ice-free Barents Sea. In contrast, during ICE– years, two geographically disconnected phytoplankton blooms are visible: one in the south and the other one close to the marginal ice zone (MIZ) located further north. With the ongoing northward and eastward shift of the MIZ, our results suggest that these blooms may follow the same geographical pattern. Differences between 2003 (maximum sea ice extent) and 2007 (minimum sea ice extent) blooms can be explained by wind stress that acts on vertical mixing. The spring bloom magnitude and length are regulated by the available nutrients at the surface. When compared to results obtained in years of large sea ice extent (e.g., 2003), years of small sea ice extent (e.g., 2007) show higher annual but lower spring Chl *a*. Large storms were recorded in late May 2003 [Pozdnyakov *et al.*, 2014] that increased the vertical mixing and entrained nutrients from the deeper layers, thereby stimulating phytoplankton growth during the last stage of the spring bloom, which explains the higher Chl *a* observed in May 2003 compared with May 2007.

In the postspring bloom period (June), low Chl *a* is retrieved in the whole Barents and for all years. However, moderate Chl *a* concentrations were observed, especially in 2007, along the outer section of the Svalbard bank and the Northern Front in June (Figure 8f). The higher annual Chl *a* estimated in 2007 was attributed to a higher occurrence/presence of summer blooms sustained by nutrients supplied by more mixing events (supporting information Figure S4). It is also known that turbulent mixing on shallow banks caused by tidal currents is an efficient mechanism to replenish nutrients in the surface layer [Le Fouest *et al.*, 2011; Fer and

Drinkwater, 2014]. These processes induce moderate Chl *a* concentrations, like in June, which can be clearly distinguished in models [e.g., *Wassmann et al.*, 2006].

4.3. The Southern Front: A Major Feature Initiating Summer Blooms

In agreement with other remote sensing studies of coccolithophores [*Signorini and McClain*, 2009; *Hopkins et al.*, 2015], our analysis reveals the presence of significant coccolithophore blooms in summer. These blooms generally peak in late July when surface waters are highly stratified, high in temperature and low in nutrients, in agreement with what is known about the ecophysiology of these species [*Paasche*, 2002; *Pasquer et al.*, 2005].

Despite an important interannual variability, the retrieved PIC bulk was located only within the Atlantic Water (Figure 2), delineated by the features of the Southern and Polar Fronts (Figure 4c). *Hovland et al.* [2014] observed the presence of coccolithophores on the Atlantic side of the Polar Front on the Svalbard bank in summer 2007. This underlies the key role of the Southern Front, a physical barrier between warm Atlantic Waters and colder Barents Sea and Arctic Waters, to delimit and predict regions of high PIC/coccolithophores in summer. Their geographical distribution will be thus concomitant to the Atlantic Water expansion. This explains why the coccolithophore summer bloom can reach east of 35°E following the northward and eastward shifts of the Southern Front during a year of low sea ice extent, whereas it remains in the southwestern Barents Sea during a year of high sea ice extent. Supporting this, coccolithophores were recorded at latitudes as high as 80°N, 30°E in 2008, a year of extreme Atlantic Water intrusion [*Hegseth and Sundfjord*, 2008].

In late August and early September, a noncalcifying phytoplankton bloom occurs mostly along the Southern Front (Figure 4b) as suggested by the increase in Chl *a* and decrease in PIC (Figure 2). This phytoplankton growth was fueled by nutrients brought to the surface by mixing caused by two distinct processes. First, the atmosphere cools and wind speed increases in late summer (see supporting information Figure S4), generating mixing of the water column by atmospheric forcing. Second, oceanic fronts like the Southern Front intensify vertical mixing in the water column [*Allen et al.*, 2005]. The hydrographic structure of the Southern Front allows Atlantic Water to “shoal” over the dense Barents Sea Water. Indeed, Atlantic Water isopycnals reaching the surface and potential vertical mixing were observed south of the Southern Front. A clear destratification was observed along the Vardø section south of the Southern Front in September 2007, where higher Chl *a* concentrations were detected. In August 2007, such enhanced frontal mixing was also reported along the Polar Front on the Great Bank slope [*Våge et al.*, 2014], as well as modest increase in Chl *a* concentration (1–2 mg/m³) on the Svalbard Bank and Great Bank [*Erga et al.*, 2014]. Accordingly, *Fer and Drinkwater* [2014] and *Randelhoff et al.* [2015] concluded that upward vertical fluxes of nitrate from deeper Atlantic Water can reach the subsurface via isopycnal transports along the Polar Front. Last, *Børshem and Drinkwater* [2014] found that primary production in the frontal region was 30% higher than in the Atlantic and Arctic Waters.

The Southern Front is not the only feature that controls summer blooms. Large amounts of melt water can negatively affect their extent and magnitude by inhibiting mixing and thus reinforcing the vertical stratification. The position of both the Southern Front, the sea ice extent, and sea ice volume seem to be critical in defining the summer mixing/stratification mechanisms. Altogether, sea ice extent and magnitude appear to have antagonistic impacts on phytoplankton spring and summer blooms (i.e., favorable on spring and negative on summer blooms).

4.4. Influence of “Atlantification” on Phytoplankton Blooms in the Barents Sea

The “Atlantification” of the Barents Sea, a direct consequence of climate change, results in a significant increase of the area occupied by the Atlantic Water and a decrease in winter sea ice cover [*Reigstad et al.*, 2002; *Rat'kova and Wassmann* 2002; *Wassmann et al.*, 2006; *Årthun et al.*, 2012; *Oziel et al.*, 2016]. Reduced amounts of melt water and stronger atmospheric forcing are therefore predicted across the Barents Sea modifying the strength of the vertical stratification and thus the nutrient supply, which dictates the different phenological regimes observed in the Arctic Ocean [*Ardyna et al.*, 2011; *Tremblay et al.*, 2015].

In this context of “Atlantification” and “Arctic Amplification” [i.e., *Screen and Simmonds*, 2010] of the Barents Sea during the coming decades, it may be expected that the ICE– case scenarios will become increasingly likely. During an ICE– year, the reduced sea ice extent allows large northward and eastward shifts of the

spring bloom (especially the ice edge bloom) with Atlantic Water intrusions. The spring bloom splits in two distinct locations: the Atlantic and Coastal Water areas and at the ice edge. The shift of the Southern Front, towards the North and East, resulting in the ongoing “Atlantification” also plays an important role in moving these summer blooms (calcifying and noncalcifying) in a similar direction. The responses of high latitude ecosystems of the northern hemisphere to the current context of receding sea ice remain highly contrasted [Mueter *et al.*, 2009; Hunt *et al.*, 2013]. Similar ecosystem regime shifts like poleward movement have been previously observed in “inflow shelves” (i.e., in the Atlantic sector [Drinkwater, 2006, 2011] and in the Bering Sea [Napp and Hunt, 2001; Grebmeier *et al.*, 2006; Mueter and Litzow, 2008]). However, these ongoing poleward shifts observed in the inflow shelves cannot be translated to “interior” (i.e., Beaufort and Russian seas) and “outflow shelves” (i.e., Baffin Bay, Canadian Archipelago, East Greenland shelf. . .), due to their entirely different functional type [Carmack and Wassmann 2006; Michel *et al.* 2015]. In the less sea-ice-covered interior shelves, stronger atmosphere-ocean interactions promote the existence of coastal hotspots of high phytoplankton productivity crucial for supporting marine ecosystems [Tremblay *et al.*, 2011; Ardyna *et al.*, 2017; Blais *et al.*, 2017]. On the contrary, outflow shelves (e.g., Baffin Bay) seem to experience drastic decrease in phytoplankton biomass and productivity [Bergeron and Tremblay, 2014; Blais *et al.*, 2017], and in the bloom magnitude [Marchese *et al.*, 2017].

In the long-term, variability in the mixing regimes may have drastic impacts on phytoplankton growth and seasonality in the changing Barents Sea. Increase in MLD may cause: (1) a delay in the occurrence of the spring bloom given that stratification is critical for its triggering, and (2) an increase in the magnitude and duration of the spring and summer blooms of noncalcifying phytoplankton. A strengthened mixing means more episodic nutrient replenishments in the surface layer. It would be conversely favorable for sustaining spring blooms and initiating summer noncalcifying phytoplankton blooms on the condition that the mixing is not too deep, allowing optimal light and temperature conditions. The current deepening of the MLD in the northern and eastern Barents Sea, where the Atlantic Water is advected in regions dominated by Arctic Water, would be a plausible hypothesis for explaining the increasing Chl *a* trend in this specific area.

However, with the decreasing nutrient content of inflowing Atlantic Water, this increasing trend in Chl *a* may be damped. A more severe nutrient limitation would favor smaller phytoplankton more adapted to oligotrophic regions [Tremblay *et al.*, 2009; Ardyna *et al.*, 2011]. The main nutrient supply mechanism in the Barents Sea would be vertical mixing, rather than advection from the Atlantic Ocean. The ocean-atmosphere interaction is additionally enhanced in the Barents Sea by the receding sea ice cover, which may amplify the importance of local nutrient replenishment. Further investigation clearly needs to be focused on quantifying the role of the mixing regimes and local nutrients replenishment that are critical for marine ecosystems of the Barents Sea, and especially in the context of decreasing Atlantic nutrient supply.

5. Conclusions

Remotely sensed Chl *a* and PIC reveal the existence of at least three distinct blooms in the Barents Sea. The spring bloom, composed exclusively of “non-calcifying” phytoplankton, is triggered by two stratification processes: surface heating in the south and sea ice melting along the MIZ in the north. The summer period is characterized by the succession of coccolithophores in late July when stratification and oligotrophic conditions are severe, followed by “non-calcifying” phytoplankton when vertical mixing increases in September.

Summer blooms seem to be tightly linked to the vertical mixing in the Atlantic Water area induced by local destratification along the mesoscale structure of the Polar and Southern Fronts combined with strong atmospheric forcing. Melt water volume also appears to be a key factor that can have a major influence by preventing vertical mixing. Finally, our interannual study suggests that in an “Atlantification” context, both spring and summer blooms are extending further North and East due to the receding ice-edge and to the shift of the Southern Front in the same directions. Annual Chl *a* and PIC concentrations have both increased during the last 17 years, whereas the winter input of nutrients from Atlantic Water at the Barents Sea entrance section (BSO) decreased. This leads to major questions about the future predictions about phytoplankton phenology and nutrient dynamics in an “Atlantified” Barents Sea: how will the decline in winter nutrient stocks will affect phytoplankton dynamics?

Acknowledgments

The research was supported by the ACCESS project (grant agreement 265863) in response to the Ocean of Tomorrow call of the European Commission 7th Framework Programme. The EU project ACCESS coordinated by the University Pierre et Marie Curie in Paris, France, provided funding for the lead author's 3 year PhD based at LOCEAN laboratory. The authors want to thank the joint contribution of the UMI Takuvik research programs and the Canada Excellence Research Chair in Remote Sensing of Canada's New Arctic Frontier. Griet Neukermans holds a Banting postdoctoral fellowship of the Canadian Government. This is also a contribution of the ARCTIC marine ecosystem research network, ARCTOS (www.arctosresearch.net) and the research project Arctic Seasonal Ice Zone Ecology (Arctic SIZÉ). The authors want to thanks Michel Crépon for his constructive advices and Debra Christiansen-Stowe for reviewing the English. The Hydrographic data were provided by the ICES Data Centre (www.ices.dk) and the Arctic and Antarctic Research Institute, Russia. The authors are particularly grateful for the Chl *a* and nutrients database shared by the IMR, Norway and for the SINMOD model that was provided by Dag Slagstad from SINTEF fisheries in Trondheim, Norway. The ERA-Interim data were obtained from the European Centre for Medium-Range Weather Forecasts data server. Ice concentration were obtained from SSM/I satellite, NSIDC, USA [NSIDC-0051]. GlobColour data (<http://globcolour.info>) used in this study was been developed, validated, and distributed by ACRI-ST, France.

References

Allen, J., L. Brown, R. Sanders, C. Moore, A. Mustard, S. Fielding, M. Lucas, M. Rixen, G. Savidge, and S. Henson (2005), Diatom carbon export enhanced by silicate upwelling in the northeast Atlantic, *Nature*, *437*, 728–732, doi:10.1038/nature03948.

Ardyna, M., M. Gosselin, C. Michel, M. Poulin, and J.-É. Tremblay (2011), Environmental forcing of phytoplankton community structure and function in the Canadian High Arctic: Contrasting oligotrophic and eutrophic regions, *Mar. Ecol. Prog. Ser.*, *44*, 37–47, doi:10.3354/meps09378.

Ardyna, M., M. Babin, M. Gosselin, E. Devred, S. Bélanger, A. Matsuoka, and J.-É. Tremblay (2013), Parameterization of vertical chlorophyll *a* in the Arctic Ocean: Impact of the subsurface chlorophyll maximum on regional, seasonal, and annual primary production estimates, *Biogeosciences*, *10*, 4383–4404, doi:10.5194/bg-10-4383-2013.

Ardyna, M., M. Babin, M. Gosselin, E. Devred, L. Rainville, and J.-É. Tremblay (2014), Recent Arctic Ocean sea ice loss triggers novel fall phytoplankton blooms, *Geophys. Res. Lett.*, *41*, 6207–6212, doi:10.1002/2014GL061047.

Ardyna, M., M. Babin, E. Devred, A. Forest, P. Raimbault, M. Gosselin, and J.-É. Tremblay (2017), Shelf-basin gradients shape ecological phytoplankton niches and community composition in the coastal Arctic Ocean (Beaufort Sea), *Limnol. Oceanogr.*, doi:10.1002/lno.10554, in press.

Arrigo, K. R., and G. L. van Dijken (2015), Continued increases in Arctic Ocean primary production, *Prog. Oceanogr.*, *136*, 60–70, doi:10.1016/j.pocean.2015.05.002.

Arrigo, K. R., G. van Dijken, and S. Pabi (2008), Impact of a shrinking Arctic ice cover on marine primary production, *Geophys. Res. Lett.*, *35*, L19603, doi:10.1029/2008GL035028.

Arrigo, K. R., et al. (2012), Massive phytoplankton blooms under Arctic sea ice, *Science*, *336*(6087), 1408–1408.

Arrigo, K. R., et al. (2014), Phytoplankton blooms beneath the sea ice in the Chukchi Sea, *Deep Sea Res., Part II*, *105*, 1–16, doi:10.1016/j.dsr2.2014.03.018.

Årthun, M., T. Eldevik, L. H. Smedsrud, Ø. Skagseth, and R. B. Ingvaldsen (2012), Quantifying the influence of Atlantic heat on Barents Sea variability and retreat, *J. Clim.*, *25*, 4736–4743, doi:10.1175/JCLI-D-11-00466.1.

Assmy, P., et al. (2017), Leads in Arctic pack ice enable early phytoplankton blooms below snow-covered sea ice, *Sci. Rep.*, *7*, 40850.

Balch, W. M., P. M. Holligan, S. G. Ackleson, and K. J. Voss (1991), Biological and optical properties of mesoscale coccolithophore blooms in the Gulf of Maine, *Limnol. Oceanogr.*, *36*(4), 629–643, doi:10.4319/lno.1991.36.4.0629.

Balch, W. M., H. R. Gordon, B. C. Bowler, D. T. Drapeau, and E. S. Booth (2005), Calcium carbonate measurements in the surface global ocean based on moderate-resolution imaging spectroradiometer data, *J. Geophys. Res.*, *110*, C07001, doi:10.1029/2004JC002560.

Bélanger, S., M. Babin, and J.-É. Tremblay (2013), Increasing cloudiness in Arctic damps the increase in phytoplankton primary production due to sea ice receding, *Biogeosciences*, *10*(6), 4087–4101, doi:10.5194/bg-10-4087-2013.

Bergeron, M., and J.-É. Tremblay (2014), Shifts in biological productivity inferred from nutrient drawdown in the southern Beaufort Sea (2003–2011) and northern Baffin Bay (1997–2011), *Canadian Arctic, Geophys. Res. Lett.*, *41*, 3979–3987, doi:10.1002/2014GL059649.

Blais, M., M. Ardyna, M. Gosselin, D. Dumont, S. Bélanger, J.-É. Tremblay, Y. Gratton, C. Marchese, and M. Poulin (2017), Contrasting interannual changes in phytoplankton productivity and community structure in the coastal Canadian Arctic Ocean, *Limnol. Oceanogr.*, doi:10.1002/lno.10581, in press.

Blindheim, J., V. Borovkov, B. Hansen, S.-A. Malmberg, W. R. Turrell, and S. Osterhus (1999), Upper layer cooling and freshening in the Norwegian Sea in relation to atmospheric forcing, *Deep Sea Res., Part I*, *47*, 655–680, doi:10.1016/S0967-0637(99)00070-9.

Borman, A. H., P. van der Wal, E. W. De Jong, and P. Westbroek (1983), Coccolith formation in *Emiliania huxleyi*, *Protistologica*, *19*, 468–469.

Børsheim, K. Y., and K. F. Drinkwater (2014), Different temperature adaptation in Arctic and Atlantic heterotrophic bacteria in the Barents Sea Polar Front region, *J. Mar. Syst.*, *130*, 160–166, doi:10.1016/j.jmarsys.2012.09.007.

Carmack, E., and P. Wassmann (2006), Food webs and physical–biological coupling on pan-Arctic shelves: Unifying concepts and comprehensive perspectives, *Prog. Oceanogr.*, *71*(2), 446–477.

Cavaliere, D. J., C. L. Parkinson, P. Gloersen, and H. J. Zwally (1996), *Sea Ice Concentrations from Nimbus-7 SMMR and DMSP SSM/I-SSMIS Passive Microwave Data, Version 1* [updated yearly], NASA Natl. Snow and Ice Data Cent. Distrib. Activ. Arch. Cent., Boulder, Colo., doi:10.5067/8GQ8LZQVLOVL.

Dalpadado, P., R. B. Ingvaldsen, L. C. Stige, B. Bogstad, T. Knutsen, G. Ottersen, and B. Ellertsen (2012), Climate effects on Barents Sea ecosystem dynamics, *ICES J. Mar. Sci.*, *69*(7), 1303–1316, doi:10.1093/icesjms/fss063.

Dalpadado, P., K. R. Arrigo, S. S. Hjøllø, F. Rey, R. B. Ingvaldsen, E. Sperfeld, G. L. van Dijken, L. C. Stige, A. Olsen, and G. Ottersen (2014), Productivity in the Barents Sea: Response to recent climate variability, *PLoS One*, *9*(5), doi:10.1371/journal.pone.0095273.

Daniels, C. J., R. M. Sheward, and A. J. Poulton (2014), Biogeochemical implications of comparative growth rates of *Emiliania huxleyi* and *Coccolithus* species, *Biogeosciences*, *11*(23), 6915–6925.

Degerlund, M. and H. C. Eilertsen (2010), Main species characteristics of phytoplankton spring blooms in NE Atlantic and Arctic Waters (68–80°N), *Estuaries Coasts*, *33*(2), 242–269, doi:10.1007/s12237-009-9167-7.

Drinkwater, K. F. (2006), The regime shift of the 1920s and 1930s in the North Atlantic, *Prog. Oceanogr.*, *68*, 134–151.

Drinkwater, K. F. (2011), The influence of climate variability and change on the ecosystems of the Barents Sea and adjacent waters: Review and synthesis of recent studies from the NESSAS Project, *Prog. Oceanogr.*, *90*, 47–61.

Ellingsen, I. H., P. Dalpadado, D. Slagstad, and H. Loeng (2008), Impact of climatic change on the biological production in the Barents Sea, *Clim. Change*, *87*, 155–175, doi:10.1007/s10584-007-9369-6.

Engelsen, O., E. N. Hegseth, H. Hop, E. Hansen, and S. Falk-Petersen (2002), Spatial variability of chlorophyll-*a* in the Marginal Ice Zone of the Barents Sea, with relations to sea ice and oceanographic conditions, *J. Mar. Syst.*, *35*, 79–97, doi:10.1016/S0924-7963(02)00077-5.

Erga, S. R., N. Ssebiyonga, B. Hamre, Ø. Frette, F. Rey, and K. F. Drinkwater (2014), Nutrients and phytoplankton distribution and activity at the Barents Sea Polar Front in summer near Hopen and Storbanken, *J. Mar. Syst.*, *130*, 181–192, doi:10.1016/j.jmarsys.2012.12.008.

Feng, Y., M. E. Warner, Y. Zhang, J. Sun, F. X. Fu, J. M. Rose, and D. A. Hutchins (2008), Interactive effects of increased pCO₂, temperature and irradiance on the marine coccolithophore *Emiliania huxleyi* (Prymnesiophyceae), *Eur. J. Phycol.*, *43*, 87–98, doi:10.1080/09670260701664674.

Fer, I., and K. Drinkwater (2014), Mixing in the Barents Sea Polar Front near Hopen in spring, *J. Mar. Syst.*, *130*, 206–218, doi:10.1016/j.jmarsys.2012.01.005.

Fischer, A., E. Moberg, H. Alexander, E. Brownlee, K. Hunter-Cevera, K. Pitz, S. Rosengard, and H. Sosik (2014), Sixty years of *Sverdrup*: A retrospective of progress in the study of phytoplankton blooms, *Oceanography*, *27*(1), 222–235.

Furevik, T. (2001), Annual and interannual variability of Atlantic Water temperatures in the Norwegian and Barents Seas: 1980–1996, *Deep Sea Res., Part I*, *48*, 383–404, doi:10.1016/S0967-0637(00)00050-9.

Giraudeau, J., V. Hulot, V. Hanquiez, L. Devaux, H. Howa, and T. Garlan (2016), A survey of the summer coccolithophore community in the western Barents Sea, *J. Mar. Syst.*, *158*, 93–105, doi:10.1016/j.jmarsys.2016.02.012.

- Gordon, H. R., G. C. Boynton, W. M. Balch, S. B. Groom, D. S. Harbour, and T. J. Smyth (2001), Retrieval of coccolithophore calcite concentration from SeaWiFS imagery, *Geophys. Res. Lett.*, **28**, 1587–1590, doi:10.1029/2000GL012025.
- Gosselin, M., M. Levasseur, P. A. Wheeler, R. A. Horner, and B. C. Booth (1997), New measurements of phytoplankton and ice algal production in the Arctic Ocean, *Deep Sea Res., Part II*, **44**, 1623–1644, doi:10.1016/S0967-0645(97)00054-4.
- Grebmeier, J. M., J. E. Overland, S. E. Moore, E. V. Farley, E. C. Carmack, L. W. Cooper, K. E. Frey, J. H. Helle, F. A. McLaughlin, and S. L. McNutt (2006), A major ecosystem shift in the northern Bering Sea, *Science*, **311**(5766), 1461–1464.
- Hegseth, E. N., and A. Sundfjord (2008), Intrusion and blooming of Atlantic phytoplankton species in the high Arctic, *J. Mar. Syst.*, **74**(1–2), 108–119, doi:10.1016/j.jmarsys.2007.11.011.
- Hibler, W. D., III (1979), A dynamic thermodynamic sea ice model, *J. Phys. Oceanogr.*, **9**(4), 815–846, doi:10.1175/1520-0485(1979)009<0815:ADTSIM>2.0.CO;2.
- Holligan, P. M., et al. (1993), A biogeochemical study of the coccolithophore, *Emiliania huxleyi*, in the North Atlantic, *Global Biogeochem. Cycles*, **7**, 879–900, doi:10.1029/93GB01731.
- Hopkins, J., S. A. Henson, S. C. Painter, T. Tyrrell, and A. J. Poulton (2015), Phenological characteristics of global coccolithophore blooms, *Global Biogeochem. Cycles*, **29**, 239–253, doi:10.1002/2014GB004919.
- Hovland, E. K., K. Hancke, M. O. Alver, K. Drinkwater, J. Høkedal, G. Johnsen, M. Moline, and E. Sakshaug (2014), Optical impact of an *Emiliania huxleyi* bloom in the frontal region of the Barents Sea, *J. Mar. Syst.*, **130**, 228–240, doi:10.1016/j.jmarsys.2012.07.002.
- Hunt, G. L., Jr., et al. (2013), The Barents and Chukchi Seas: Comparison of two Arctic shelf ecosystems, *J. Mar. Syst.*, **109–110**, 43–68.
- Ivanov, V., A. Korablev, and O. Myakoshin (1996), PC-adapted oceanographic database for studying climate shaping ocean processes, in *Oceanology International 96, The Global Ocean-Towards Operational Oceanography, Conference Proceedings*, vol. 1, pp. 89–99, Spearhead Exhib. Ltd, New Malden, U. K.
- Johannesen, E., R. B. Ingvaldsen, P. Dalpadado, M. Skern-Mauritzen, J. E. Stiansen, E. Eriksen, H. Gjøsæter, B. Bogstad, and T. Knutsen (2012), The Barents Sea ecosystem state 1970–2009: Climate fluctuations, human impact and trophic interactions, *ICES J. Mar. Sci.*, **69**(5), 880–889, doi:10.1093/icesjms/fss046.
- Kogeler, J., and F. Rey (1999), Ocean colour and the spatial and seasonal distribution of phytoplankton in the Barents Sea, *Int. J. Remote Sens.*, **20**, 1303–1318, doi:10.1080/014311699212740.
- Korablev, A., A. Pnyushkov, and A. Smirnov (2007), Compiling of the oceanographic database for climate monitoring in the Nordic Seas [in Russian], *Trudy AARI*, **447**, 85–108.
- Le Fouest, V., C. Postlethwaite, M. A. M. Maqueda, S. Belanger, and M. Babin (2011), On the role of tides and strong wind events in promoting summer primary production in the Barents Sea, *Cont. Shelf Res.*, **31**(17), 1869–1879, doi:10.1016/j.csr.2011.08.013.
- Le Quééré, C., et al. (2005), Ecosystem dynamics based on plankton functional types for global ocean biogeochemistry models, *Global Change Biol.*, **11**, 2016–2040, doi:10.1111/j.1365-2486.2005.01004.x.
- Loeng, H. (1991), Features of the physical oceanographic conditions of the Barents Sea, *Polar Res.*, **10**, 5–18, doi:10.1111/j.1751-8369.1991.tb00630.x.
- Loeng, H., and K. Drinkwater (2007), An overview of the ecosystems of the Barents and Norwegian Seas and their response to climate variability, *Deep Sea Res., Part II*, **54**, 2478–2500, doi:10.1016/j.dsr2.2007.08.013.
- Marchese, C., C. Albouy, J.-É. Tremblay, D. Dumont, F. D'Ortenzio, S. Vissault, and S. Bélanger (2017), Changes in phytoplankton bloom phenology over the North Water (NOW) polynya: A response to changing environmental conditions, *Polar Biol.*, 1–17, doi:10.1007/s00300-017-2095-2.
- Maritorena, S., O. H. F. d'Andon, A. Mangin, and D. A. Siegel (2010), Merged satellite ocean color data products using a bio-optical model: Characteristics, benefits and issues, *Remote Sens. Environ.*, **114**(8), 1791–1804, doi:10.1016/j.rse.2010.04.002.
- Michel, C., J. Hamilton, E. Hansen, D. Barber, M. Reigstad, J. Iacozza, L. Seuthe, and A. Niemi (2015), Arctic Ocean outflow shelves in the changing Arctic: A review and perspectives, *Prog. Oceanogr.*, **139**, 66–88.
- Mitchell, B., E. A. Brody, E. N. Yeh, C. McClain, J. Comiso, and N. G. Maynard (1991), Meridional zonation of the Barents Sea ecosystem inferred from satellite remote sensing and in situ bio-optical observations, *Polar Res.*, **10**(1), 147–162, doi:10.1111/j.1751-8369.1991.tb00641.x.
- Morel, A., Y. Huot, B. Gentili, P. J. Werdell, S. B. Hooker, and B. A. Franz (2007), Examining the consistency of products derived from various ocean color sensors in open ocean (Case 1) waters in the perspective of a multi-sensor approach, *Remote Sens. Environ.*, **111**(1), 6988, doi:10.1016/j.rse.2007.03.012.
- Moore, T. S., M. D. Dowell, and B. A. Franz (2012), Detection of coccolithophore blooms in ocean color satellite imagery: A generalized approach for use with multiple sensors, *Remote Sens. Environ.*, **117**, 249–263, doi:10.1016/j.rse.2011.10.001.
- Mueter, F. J., and M. A. Litzow (2008), Sea ice retreat alters the biogeography of the Bering Sea continental shelf, *Ecol. Appl.*, **18**(2), 309–320.
- Mueter, F. J., C. Broms, K. F. Drinkwater, K. D. Friedland, J. A. Hare, G. L. Hunt, W. Melle, and M. Taylor (2009), Ecosystem responses to recent oceanographic variability in high-latitude Northern Hemisphere ecosystems, *Prog. Oceanogr.*, **81**(1), 93–110.
- Mundy, C. J., et al. (2009), Contribution of under-ice primary production to an ice-edge upwelling phytoplankton bloom in the Canadian Beaufort Sea, *Geophys. Res. Lett.*, **36**, L17601, doi:10.1029/2009GL038837.
- Napp, J. M., and G. L. Hunt (2001), Anomalous conditions in the south-eastern Bering Sea 1997: Linkages among climate, weather, ocean, and Biology, *Fish. Oceanogr.*, **10**(1), 61–68.
- Nilsen, J. E. Ø., H. Hátún, K. A. Mork, and H. Valdimarson (2008), The NISE dataset, *Tech. Rep.*, 07–01, Faroese Fish. Lab., Tórshavn, Faroe Islands.
- Overland, J. E., M. Wang, K. R. Wood, D. B. Percival, and N. A. Bond (2012), Recent Bering Sea warm and cold events in a 95-year context, *Deep Sea Res., Part II*, **65–70**, 6–13, doi:10.1016/j.dsr2.2012.02.013.
- Oziel, L., J. Sirven, and J.-C. Gascard (2016), The Barents Sea frontal zones and water masses variability (1980–2011), *Ocean Sci.*, **12**(1), 169–184, doi:10.5194/os-12-169-2016.
- Paasche, E. (2002), A review of the coccolithophorid *Emiliania huxleyi* (Prymnesiophyceae), with particular reference to growth, coccolith formation, and calcification-photosynthesis interactions, *Phycologia*, **40**, 503–529, doi:10.2216/i0031 8884-40-6-503.1.
- Pasquer, B., G. Laruelle, S. Becquevort, V. Schoemann, H. Goosse, and C. Lancelot (2005), Linking ocean biogeochemical cycles and ecosystem structure and function: Results of the complex SWAMCO-4 model, *J. Sea Res.*, **53**(1), 93–108, doi:10.1016/j.seares.2004.07.001.
- Peralta-Ferriz, C., and R. A. Woodgate (2014), Seasonal and interannual variability of pan-Arctic surface mixed layer properties from 1979 to 2012 from hydrographic data, and the dominance of stratification for multiyear mixed layer depth shoaling, *Prog. Oceanogr.*, **134**, 19–53, doi:10.1016/j.pocan.2014.12.005.
- Polyakov, I. V., et al. (2017), Greater role for Atlantic inflows on sea-ice loss in the Eurasian Basin of the Arctic Ocean, *Science*, **356**(6335), 285–291, doi:10.1126/science.aai8204.
- Pozdnyakov, D., D. Tang, L. Bobylev, P. Golubkin, E. Zabolotskikh, D. Petrenko, and E. Morozov (2014), A pilot satellite-based investigation of the impact of a deep polar cyclone propagation on the phytoplankton chlorophyll spatial and temporal dynamics in the Arctic

- Ocean, in *Typhoon Impact and Crisis Management, Advances in Natural and Technological Hazards Research*, edited by D. L. Tang and G. J. Sui, pp. 241–251, Springer, Berlin, doi:10.1007/978-3-642-40695-9_11.
- Qu, B., A. J. Gabric, and P. A. Matrai (2006), The satellite-derived distribution of chlorophyll-a and its relation to ice cover, radiation and sea surface temperature in the Barents Sea, *Polar Biol.*, *29*(3), 196–210, doi:10.1007/s00300-005-0040-2.
- Randelhoff, A., A. Sundfjord, and M. Reigstad (2015), Seasonal variability and fluxes of nitrate in the surface waters over the Arctic shelf slope, *Geophys. Res. Lett.*, *42*, 3442–3449, doi:10.1002/2015GL063655.
- Rat'kova, T. N., and P. Wassmann (2002), Seasonal variation and spatial distribution of phyto- and protozooplankton in the central Barents Sea, *J. Mar. Syst.*, *38*, 47–75, doi:10.1016/S0924-7963(02)00169-0.
- Reigstad, M., P. Wassmann, C. W. Riser, S. Øygarden, and F. Re (2002), Variations in hydrography, nutrients and chlorophyll a in the marginal ice-zone and the central Barents Sea, *J. Mar. Syst.*, *38*(1–2), 9–29, doi:10.1016/S0924-7963(02)00167-7.
- Reigstad, M., J. Carroll, D. Slagstad, I. Ellingsen, and P. Wassmann (2011), Intra-regional comparison of productivity, carbon flux and ecosystem composition within the northern Barents Sea, *Prog. Oceanogr.*, *90*(1–4), 33–46, doi:10.1016/j.pocean.2011.02.005.
- Rey, F. (2004), Phytoplankton: The grass of the sea, in *The Norwegian Sea Ecosystem*, edited by H. R. Skjoldal, pp. 97–136, Tapir Academic Press, Trondheim, Norway.
- Rey, F. (2012), Declining silicate concentrations in the Norwegian and Barents Seas, *ICES J. Mar. Sci.*, *69*(2), 208–212, doi:10.1093/icesjms/ffs007.
- Sakshaug, E. (2004), Primary and secondary production in the Arctic Seas, in *The Organic Carbon Cycle in the Arctic Ocean*, edited by R. Stein and R. Macdonald, pp. 57–81, Springer, Berlin, doi:10.1007/978-3-642-18912-8_3.
- Sakshaug, E., and H. R. Skjoldal (1989), Life at the ice edge, *Ambio*, *18*, 60–67.
- Screen, J. A., and I. Simmonds (2010), The central role of diminishing sea ice in recent Arctic temperature amplification, *Nature*, *464*, 1334–1337, doi:10.1038/nature09051.
- Serreze, M., and R. Barry (2011), Processes and impacts of Arctic Amplification, *Global Planet. Change*, *77*(1–2), 85–96, doi:10.1016/j.gloplacha.2011.03.004.
- Signorini, S. R., and C. R. McClain (2009), Environmental factors controlling the Barents Sea spring-summer phytoplankton blooms, *Geophys. Res. Lett.*, *36*, L10604, doi:10.1029/2009GL037695.
- Slagstad, D., and P. Wassmann (1996), Climatic change and carbon flux in the Barents Sea: 3-D simulations of ice-distribution, primary production and vertical export of particulate organic carbon, *Mem. Natl. Inst. Polar Res., Spec. Issue*, *51*, 119–141.
- Slagstad, D., P. F. J. Wassmann, and I. Ellingsen (2015), Physical constrains and productivity in the future Arctic Ocean, *Front. Mar. Sci.*, *2*, 1–23, doi:10.3389/fmars.2015.00085.
- Smedsrud, L. H., et al. (2013), The role of the Barents Sea in the Arctic Climate System, *Rev. Geophys.*, *51*, 415–449, doi:10.1002/rog.20017.
- Smyth, T. J., T. Tyrell, and B. Tarrant (2004), Time series of coccolithophore activity in the Barents Sea, from twenty years of satellite imagery, *Geophys. Res. Lett.*, *31*, L11302, doi:10.1029/2004GL019735.
- Stroeve, J. C., T. Markus, L. Boisvert, J. Miller, and A. Barrett (2014), Changes in Arctic melt season and implications for sea ice loss, *Geophys. Res. Lett.*, *41*, 1216–1225, doi:10.1002/2013GL058951.
- Sverdrup, H. (1953), On conditions for the vernal blooming of phytoplankton, *J. Con. Int. Explor. Mer.*, *18*, 287–295, doi:10.1093/icesjms/18.3.287.
- Tremblay, G., C. Belzile, M. Gosselin, M. Poulin, S. Roy, and J.-É. Tremblay (2009), Late summer phytoplankton distribution along a 3500 km transect in Canadian Arctic waters: Strong numerical dominance by picoeukaryotes, *Aquat. Microb. Ecol.*, *54*, 55–70.
- Tremblay, J.-É., et al. (2011), Climate forcing multiplies biological productivity in the coastal Arctic Ocean, *GRL* *38*.
- Tremblay, J. É., L. G. Anderson, P. Matrai, P. Coupel, S. Bélanger, C. Michel, and M. Reigstad (2015), Global and regional drivers of nutrient supply, primary production and CO₂ drawdown in the changing Arctic Ocean, *Prog. Oceanogr.*, *139*, 171–196, doi:10.1016/j.pocean.2015.08.009.
- Våge, S., S. L. Basedow, K. S. Tande, and M. Zhou (2014), Physical structure of the Barents Sea Polar Front near Storbanken in August 2007, *J. Mar. Syst.*, *130*, 256–262, doi:10.1016/j.jmarsys.2011.11.019.
- Wassmann, P., M. Vernet, B. G. Mitchell, and F. Rey (1990), Mass sedimentation of *Phaeocystis pouchetii* in the Barents Sea, *Mar. Ecol. Prog. Ser.*, *66*, 183–195, doi:10.3354/meps066183.
- Wassmann, P., R. Peinert, and V. Smetacek (1991), Patterns of production and sedimentation in the boreal and polar Northeast Atlantic, *Polar Res.*, *10*(1), 209–228, doi:10.1111/j.1751-8369.1991.tb00647.x.
- Wassmann, P., T. Ratkova, I. Andreassen, M. Vernet, G. Pedersen, and F. Rey (1999), Spring bloom development in the marginal ice zone and the central Barents Sea, *Mar. Ecol.*, *20*(3–4), 321–346, doi:10.1046/j.1439-0485.1999.2034081.x.
- Wassmann, P., et al. (2006), Food webs and carbon flux in the Barents Sea, *Prog. Oceanogr.*, *71*, 232–287, doi:10.1016/j.pocean.2006.10.003.
- Wassmann, P., D. Slagstad, and I. Ellingsen (2010), Primary production and climatic variability in the European sector of the Arctic Ocean prior to 2007: Preliminary results, *Polar Biol.*, *33*(D), 1641–1650, doi:10.1007/s00300-010-0839-3.
- Westbroek, P., J. R. Young, and K. Linschooten (1989), Coccolith production (biomineralization) in the marine alga *Emiliania huxleyi*, *J. Protozool.*, *36*, 368–373, doi:10.1111/j.1550-7408.1989.tb05528.x.